Master's thesis

NTNU
Norwegian University of Science and Technology
Faculty of Engineering
Department of Energy and Process Engineering

Stian Ranøyen Bratsberg

Experimental investigation of carbon nanotube photo ignition for combustion in ICEs

Master's thesis in Energy and Environmental Engineering
Supervisor: Terese Løvås
Co-supervisor: David Emberson and Karl Oskar Pires Bjørgen
June 2022

NTNU
Norwegian University of
Science and Technology

Stian Ranøyen Bratsberg

Experimental investigation of carbon nanotube photo ignition for combustion in ICEs

Master's thesis in Energy and Environmental Engineering
Supervisor: Terese Løvås
Co-supervisor: David Emberson and Karl Oskar Pires Bjørgen
June 2022

Norwegian University of Science and Technology
Faculty of Engineering
Department of Energy and Process Engineering

Problem description

When carbon nanotubes (CNTs) are irradiated with a high intensity light, such as a camera flash, they ignite and burn – a phenomena called photo ignition. This masters project fits in to a larger project with the main objective to develop and build a new engine concept using the photo ignition of CNTs to ignite ammonia. Initial testing of CNT ignition is being conducted in a constant volume chamber, using gaseous mixtures of methane and air. This chamber is used to examine CNT delivery and the light system to be used. The objectives for this project work are summarized here, while a detailed description will be given in the main part of the thesis.

- Conduct experiments to find a suitable light source for photo ignition within a combustion chamber.
- Determine the energy required to ignite samples of CNTs and ferrocene within the combustion chamber.
- Design and optimize a method for injecting samples of CNTs and ferrocene into the combustion chamber.
- Investigate the possibility of successful photo ignition of a air-fuel mixture, using a Xe flash placed outside of the chamber.

Preface

This thesis is the conclusion of a five year Master's program within Energy and Environmental Engineering, with a specialization in Energy and Process Engineering, at the Norwegian University of Science and Technology. I am thankful for the opportunity to increase my theoretical and experimental knowledge and skills within such an interesting field as photo ignition.

I sincerely thank my supervisor, Karl Oskar Pires Bjørgen, for his practical and theoretical guidance in the lab. Without his presence and availability in the lab, I would not have gotten this far with the thesis. I would also like to thank my other supervisor, David Emberson, for guidance and suggestions that led to the success of the project. Final thanks goes to my fellow colleague at the lab, Patrick Ruvedel-Flor Heian Jørgensen, for constructive and interesting discussions and for making the hard times in the lab enjoyable.

Abstract

This work is part of the NanoIgnite project designed to investigate the possibility of igniting fuel, such as hydrogen or ammonia, in an engine using the phenomenon of photo ignition of carbon nanotubes. Initial testing examined the use of different light sources and different carbon nanotubes mixtures. It was concluded that the most powerful Xe flash was a Godox Xe camera flash. This light source was able to ignite samples of CNTs and ferrocene at distances of maximum 5.4 cm. The majority of the work presented in this thesis is the investigation using Xenon (Xe) flashes for photo ignition of an air-methane mixture within a static combustion chamber. Successful photo ignition within the static combustion chamber was achieved for samples of CNTs and ferrocene placed inside of the optical access of the chamber. To the authors' knowledge, this is the first successful photo ignition using a light source placed outside of the combustion chamber. Photo ignition did not occur for a quasi-homogeneously dispersed sample. The photo ignition's upper and lower limits for the pressure, p, and fuel-air equivalence ratio, ϕ, were respectively p=4 bar and ϕ=0.8, and p=2 bar and ϕ=0.7. Due to time constraints, relatively few experiments were conducted investigating the photo ignition. Nevertheless, a functional experimental rig for conducting further experiments concerning the phenomenon photo ignition has been created.

Sammendrag

Denne masteroppgaven er en del av prosjektet NanoIgnite, der målet er å undersøke mulighet for å antenne alternative drivstoff, slik som ammoniakk eller hydrogen, ved bruk av fotoantenning av nanorør av karbon. Det ble tidlig undersøkt mengden energi som kreves for antenning av en sammensetning av ferrocen og nanorør av karbon, ved ulike typer sammensetninger og ved bruk av ulike lyskilder. En Godox kamerablits ble konkludert med å være den mest kraftfulle lyskilden, og er i stand til å antenne blandingen av nanorør av karbon og ferrocen 5.4 cm inn i forbrenningskammeret. Lyset ble tilført partiklene gjennom et vindu i kammeret. Mesteparten av denne oppgaven omhandler bruk av Xenonlamper, for å kunne antenne en gassblanding av luft og metan i et statisk forbrenningskammer. Vellykket fotoantenning av luft og metanblandingen oppsto når sammensetningen av ferrocen og nanorør av karbon ble plassert rett innenfor vinduet. Så vidt forfatteren vet, er dette første gang fotoantenning finner sted ved bruk av en lyskilde plassert utenfor et forbrenningskammer. Sammensetningen av ferrocen og nanorør av karbon antente ikke luft og metanblandingen når partiklene var spredt i kammeret. Øvre og nedre grense for trykket, p, og det inverse luftoverskuddtallet, ϕ, i forbrenningskammeret som ledet til vellykket fotoantenning var henholdsvis p=4 bar og ϕ=0.8, i tillegg til p=2 bar og ϕ=0.7. Tidsbegrensninger førte til at det ble gjennomført få eksperimenter som omhandlet fotoantenning. Som et resultat av dette prosjektet, står man allikevel igjen med en eksperimentell rigg satt opp for å kunne utføre detaljerte undersøkelser av fenomenet fotoantenning av nanorør av karbon.

Contents

Problem description i

Preface ii

Abstract iii

Sammendrag iv

List of figures vii

List of tables ix

1 Introduction 1
- 1.1 Background . . . 1
- 1.2 Objective . . . 2
- 1.3 Previous work . . . 3

2 Theory 4
- 2.1 Carbon nanotubes . . . 4
- 2.2 Xenon lamps . . . 6
- 2.3 Driver . . . 8
- 2.4 Combustion and chamber physics . . . 9
- 2.5 Photo ignition of air-fuel mixtures . . . 13

3 Methodology 14
- 3.1 Light sources . . . 14
- 3.2 Experimental setup . . . 14
  - 3.2.1 Combustion chamber . . . 14
  - 3.2.2 Filming injection of CNTs . . . 16
  - 3.2.3 Measurement of fluence . . . 17
  - 3.2.4 CNTs and ferrocene . . . 19
  - 3.2.5 Ignition outside of the combustion chamber . . . 19
  - 3.2.6 Ignition within the combustion chamber . . . 20
- 3.3 Driver . . . 22
- 3.4 OACIC mount . . . 23
- 3.5 Health, safety and environment . . . 26

4 Results and discussion 27

4.1 Xe lamp tests . . . 27
4.2 Injection . . . 28
4.3 Ignition . . . 31
4.3.1 Outside of the combustion chamber . . . 31
4.3.2 Within the combustion chamber . . . 33

5 Conclusion **50**

6 Further work **51**

Appendices **55**

A Static combustion chamber **55**
A.1 Setup . . . 55
A.2 Performance report . . . 56

B OACIC **57**

C Experimental setup for testing of camera flash **58**

D Script for computing optimum flash delay **61**

List of Figures

1 Ignition threshold for different wavelengths [38]. 7
2 A typical flash circuit. 8
3 Effect of pressure and temperature on MIE for an air-methane mixture at ϕ=1.0. . . 11
a Effect of pressure on MIE [13]. 11
b Effect of temperature on MIE [13]. 11
4 A typical pressure development and combustion processes for a static combustion chamber. 12
5 Photo ignition pressure developments for a range of ϕ at p=3 bar [8]. 13
6 Combustion chamber used for ignition of CNTs. 15
7 System for injecting samples of CNTs and ferrocene into the combustion chamber. . 16
8 Experimental setup for filming the injection of CNTs. 17
9 Experimental setup for fluence measurements for Xe lamps. 18
10 Experimental setup for ignition of CNTs outside combustion chamber. 20
11 Experimental setup for ignition of CNTs within combustion chamber. 21
12 Mount for the camera flash. 21
13 Circuit board box. 23
a Circuit box open. 23
b Circuit box closed. 23
14 Mount for OACIC. 24
a Mount for OACIC seen from the top. 24
b Mount for OACIC seen from the bottom. 24
15 Tools designed to mount Xe lamp onto the OACIC. 25
a Mount for the reflector. 25
b Reflector for the Xe lamp. 25
16 Comparison of different Xe flashes. 27
17 A selection of the experiments where the effect of varying the tube diameter, in addition to the amount of CNTs and ferrocene, on dispersion. 30
a Injection test using sample weight of 12 mg at N_2 equal to 2 bar using medium tube. 30
b Injection test using sample weight of 24 mg at N_2 equal to 2 bar using medium tube. 30
c Injection test using sample weight of 36 mg CNT at N_2 equal to 2 bar using medium tube. 30
d Injection test using sample weight of 24 mg at N_2 equal to 4 bar using large tube. 30

e Injection test using sample weight of 24 mg at N_2 equal to 2 bar using large tube. . . . 30
f Injection test using sample weight of 12 mg at N_2 equal to 2 bar using large tube. . . . 30
18 CNTs dispersed in front of quartz glass a given amount of time after opening of injection solenoid valve, using ϕ=1.0 and p=4 bar. . . . 36
a After 0 ms . . . 36
b After 29 ms . . . 36
c After 113 ms . . . 36
d After 205 ms . . . 36
19 Experimental setup for both glass plate and basket. . . . 38
20 Development of combustion using photo ignition at ϕ=0.8 and p=4 bar and sample weight of 36 mg, in experiment 18. . . . 41
a Before trigger - 0 ms . . . 41
b Flash triggered - 3 ms . . . 41
c After trigger - 37 ms . . . 41
d Flame development phase - 63 ms . . . 41
e Flame propagation phase - 315 ms . . . 41
f Flame termination phase - 800 ms . . . 41
21 Combustion phases using photo ignition at p=4 bar and ϕ=0.8. Pressure development is given in absolute pressure. . . . 42
22 7 experiments conducted for combustion using spark ignition at p=4 bar and ϕ=0.8. Pressure developments are given in absolute pressure. . . . 43
23 Photo ignition dependence on weight of CNTs/ferrocene sample and ϕ, at p=4 bar. Pressure developments are given in absolute pressure. . . . 44
24 Comparison of photo ignition and average spark ignition at p=4 bar and ϕ=0.8. Pressure developments are given in absolute pressure. . . . 45
25 Comparison of photo ignition using injection of synthetic air and nitrogen at p=4 bar and ϕ=0.8. Pressure developments are given in absolute pressure. . . . 48
26 The static combustion chamber and its optical access. . . . 55
27 Illustration of the OACIC. . . . 57
28 Experimental setup for testing of camera flash. . . . 59
a Coordinates for investigating fluence from camera flash. . . . 59
b Measuring fluence in θ-direction. . . . 59
c Measuring fluence in ψ-direction in the yz-plane. . . . 59
d Measuring fluence in ψ-direction in the xz-plane. . . . 59

List of Tables

1 Experimental results of igniting CNT using a Xe lamp, pulsed LED, and pulsed laser. 6
2 Key features for Xe lamps used for this project. 14
3 Uncertainty in sample weight. 19
4 Experimental results of igniting CNT using a round Xe lamp. 31
5 Experimental results of igniting CNT using a Xe camera flash. 31
6 Experimental results of comparing different methods for mixing CNTs and ferrocene. 32
7 Chronological development of experiments within the combustion chamber. No value in photo ignition column refers to an experiment which was not conducted, but is strongly suggested to conduct in further experiments. Sample placements will be given in detail in this section. 34
8 Comparison of peak pressure and ignition delay for combustions at ϕ=0.8 and p=4 bar. Pressures are given as pressure above the absolute pressure. 45
9 Parameters obtained from SI experiments, conducted at p=4 bar and ϕ=0.8. 56
10 Parameters obtained from SI experiments, conducted at p=2 bar with a range of ϕ. . 56
11 Measurement of fluence at different angles for the camera flash tube. 59

Nomenclature

Abbreviations

AFR	Air-fuel ratio
$APSWCNT$	As-prepared single walled carbon nanotubes
fps	Frames per second
$HCCI$	Homogeneous charge compression ignition
$HEPA$	High efficiency particulate air
HSE	Health, safety and environment
ICE	Internal combustion engine
LD	Laser diode
LED	Light emitting diode
LPG	liquefied petroleum gas
MIE	Minimum ignition energy
$MWCNT$	Multi-walled carbon nanotubes
$NTNU$	Norges teknisk-naturvitenskapelige universitet
$OACIC$	Optically accessible compression ignition combustion chamber
p	Initial combustion chamber pressure
SI	Spark ignition
$SWCNT$	Single-walled carbon nanotubes
$Synair$	Synthetic air

Chemical symbols

CH_4	Methane
CO	Carbon monoxide

CO_2	Carbon dioxide
Fe	Iron
N_2	Nitrogen
NO_x	Nitric oxides
O_2	Oxygen
Xe	Xenon

1 Introduction

1.1 Background

In 2021, the world leaders gathered in Glasgow to find a common strategy to solve the earth's climate crisis. Most scientists agree that a global temperature rise of 2.0°C should not be exceeded, compared to pre-industrial levels, to avoid changing the climate dramatically [35].

The shipping industry emits 3 % of the annual greenhouse gases [21]. A lot of the goods nowadays are transported by large cargo ships. There has been some progress to reduce the emissions from these ships, such as investigating the possibility of using hydrogen or ammonia as possible fuels. One of the advantages of using ammonia instead of hydrogen is the pressure of storage. It is possible to store ammonia as liquid at 10 bar, while hydrogen would require a pressure between 350 and 700 bar [3].

Although there are a lot of positive effects of using ammonia in an engine, there are also some obstacles which needs to be overcome. One of those are the low laminar flame speed, equal to 0.15 m/s, in a mixture with air. This is for example approximately 4 times slower than for methane [16, 20]. This would lead to incomplete combustion. To deal with this, one possible solution is to inject carbon nanotubes (CNTs) into the combustion chamber.

If CNTs were injected and dispersed evenly into an engine, and thereafter ignited by a flash of light, one could ensure a homogeneous ignition. If the mixture in a combustion chamber is lean, a homogeneous combustion would produce a soot-free exhaust, in addition to have reduced nitric oxides (NO_x) and carbon monoxide (CO) particles in the exhaust, compared to an in-homogeneous combustion [5]. Successful photo ignition using the nanoparticles could ease the development of photo ignition engines, which would be similar to homogeneous charge compression ignition (HCCI) engines. Shortly described, HCCI engines will theoretically deliver a self-ignition of the fuel by compression and heat, which would occur at several locations within the engine. This scientific progress could decrease the consumption of fuel and immensely improve the opportunity of using ammonia in an internal combustion engine (ICE).

Single-walled carbon nanotubes (SWCNTs) and multi-walled carbon nanotubes (MWCNTs) are both allotropes of carbon. These structures are hollow cylinders made up of carbon lattices. The difference between SWCNT and MWCNT is that the latter are made up of several SWCNTs with different diameters. One nanotube has typically a diameter of 1 nm to 2 nm. The possibility of igniting SWCNTs using a flash was firstly discovered by accident in 2002 [2]. There have later been done several studies regarding different aspects of the ignition of CNTs.

Since the discovery of CNTs igniting due to a flash of light, scientists have tried to understand the chain of reaction for the ignition. Additionally, previous studies have shown how the minimum

ignition energy (MIE) depends on light source [37], type of CNT [34] and light pulse duration [4]. It has also been done multiple successful ignitions of different fuels within an engine, using the combination of CNTs and a light source as the ignition agent [5, 8, 9].

1.2 Objective

What has yet to be investigated, is a proper method to deliver luminous energy into an engine, to continuously ignite CNTs and thus the fuel. This project will investigate if Xe lamps have the required attributes to create an engine running on a fuel, where the combustion is initiated by photo ignition of nanoparticles.

The sub objective for this thesis would be to study CNT ignition using Xe flashes. In order to do so, an experimental research focusing on measurements of the available light sources needs to be conducted. Additionally, the MIE of different samples containing CNTs and ferrocene should be investigated.

When the ignition characteristics of the sample of CNT and ferrocene outside of the static combustion chamber is understood, a method for injecting the sample into the chamber should be developed. This injection system would be designed such that the probability of igniting the particles and thereafter the air-methane mixture within the chamber, should be maximized. The experimental method for doing this, would be to firstly design a secure and effective system for injecting the nanoparticles.

Secondly, an investigation of different configurations for injection of nanoparticles into the chamber should be conducted. Characteristics such as injection pressure, mass of nanoparticles, the injection tube properties and the flash trigger delay should be considered.

After building up a good knowledge of the ignition and injection characteristics of the CNTs, a study regarding combustion of methane and air using photo ignition of CNTs should be conducted. By successfully igniting the aforementioned mixture within the combustion chamber, using a light source situated outside of the chamber, a long leap towards an ammonia fueled ICE using photo ignition would be achieved. Not only would this important scientific progress be obtained, but to the authors' knowledge, the first successful photo ignition with a light source outside of a combustion chamber in history will be performed.

Even though this thesis will rely heavily on the static combustion chamber being used for experiments, a fellow master's student will have the responsibility for the main operation and investigation for this chamber. For an extensive study of the static combustion chamber, the mentioned thesis should be studied [17].

If the photo ignition succeeds using the static combustion chamber and time is still available, ex-

periments should be conducted using NTNU's optically accessible compression ignition combustion chamber (OACIC).

1.3 Previous work

The experimental work focusing on investigating suitable light sources started last semester, in the autumn of 2021. The main focus area was to investigate if light emitting diodes (LEDs) or laser diodes (LDs) did deliver a sufficient amount of energy, in order to ignite samples of CNTs and ferrocene within a combustion chamber. There are some advantages using these types of light sources, compared to for example a Xe flash.

A LED will be able to repeat a flash at a high rate, and have some other promising aspects as for example longevity. It has also been done successful research concerning the ignition of CNTs using LEDs [36]. One of the problems with this specific light source is that it delivers a smaller luminous energy each flash, compared to the camera flash.

Moreover, lasers have been proven to ignite the nanoparticles successfully in previous studies [33]. A LD offers some of the advantages of a laser, at a lower cost. It does not deliver as much energy as some lasers, but on the other hand, it could be more effective compared to a LED.

After thoroughly testing, it was made clear that both LEDs and LDs did not deliver a required amount of energy in order to ignite the particles within the combustion chamber. Therefore, more powerful light sources, such as Xe flash tubes needs to be investigated. Although, other disadvantages appears using these, as for example repetition rate and longevity.

2 Theory

2.1 Carbon nanotubes

Ajayan et al. observed that SWCNTs ignited by a light pulse generated by a camera flash [2]. Temperatures between 1500°C and 2000°C were reported in the combustion of these particles. The reaction was believed to be due to a photoacoustic effect. This occurs when the CNTs absorbs incident light, where expansion and contraction of trapped gases in turn leads to acoustic waves [12]. Kang et al. later developed the idea further. They postulated that the reaction relied on a combination of the photoacoustic response of the CNTs and the lack of dissipation of heat, as the mechanism of the ignition [18].

Several studies were conducted later to investigate this phenomenon. It was found that there was not only the SWCNTs that had the ability to ignite upon a camera flash, but also other carbonaceous mixtures [6]. Braidy et al. discovered that iron impurities i.e., Fe_2O_3 and Fe_2O_4, were present in the samples of SWCNTs [7]. They managed to prove that the Fe particles had melted during the combustion. Hence, the temperature of the combustion had been proven to be at least 1500°C, since this is the minimum temperature to melt the iron oxide.

Moving further, the importance of a metal catalyst mixed with the SWCNTs to ignite, was discovered [29]. An experiment equal to Ajayan et al. was conducted, but the result was an unsuccessful ignition of purified SWCNTs. Therefore, it was concluded that the impurities in the nanotubes were the ignition agent. The authors suggested that the photons from the light source were absorbed by the Fe particles and then converted into thermal energy, resulting in high temperatures.

While assuming that the metal catalyst was the main ignition agent, Sysoev et al. postulated a chain of reaction leading to the CNTs igniting [32]. Firstly, the metal catalyst dispersed within the CNTs oxidizes, leading to heating due to chemical reactions. One part of the energy released from this process is absorbed by the CNTs, which in turn increases the temperature of the nanotubes. The rest of the energy is lost due to heat exchange with the environment and radiation. Finally, the result of the heating of the CNTs leads to an explosion, which comes from the combustion initiated by different ignited segments within the sample. Eq. 1 shows the oxidation reactions for the combustions of CNTs and ferrocene [32].

$$\begin{aligned} \mathrm{C} + \mathrm{O_2} &\longrightarrow \mathrm{CO_2} \\ \mathrm{C} + 0.5\,\mathrm{O_2} &\longrightarrow \mathrm{CO} \\ 3\,\mathrm{Fe} + 2\,\mathrm{O_2} &\longrightarrow \mathrm{FE_2O_4} \\ 4\,\mathrm{Fe} + 3\,\mathrm{O_2} &\longrightarrow 2\,\mathrm{FE_2O_3} \end{aligned} \tag{1}$$

In 2007, Tseng et al. investigated the ignition characteristics of carbon nanotubes [34]. It was found that the nanotubes which required the least amount of energy to ignite was the "fluffy" SWCNTs, followed by "fluffy" MWCNTs. Here, the term "fluffy" is used for low density powder. Additionally, they also managed to ignite compacted SWCNT and purified SWCNT, with the compact nanotubes being the most reactive of those two. One important thing to note here, is that Tseng et al. managed to ignite purified SWCNT, while Smits et al. did not successfully ignite this type of CNTs [29].

For the case of ignition of MWCNTs, Malec et al. explored the possibility of igniting the nanotubes by adding ferrocene [19]. When the metal catalyst was not mixed with the nanotubes, the ignition using a Xe camera flash was unsuccessful. On the contrary, when adding ferrocene, combustion took place. Later it was discovered that the least luminous energy required delivered by a LED pulse, to ignite the mixture of MWCNTs and ferrocene, was a 4:1 and 2:1 weight ratio [36]. Furthermore, Primiceri et al. reported that the weight ratio used to ignite the MWCNTs/ferrocene mixture most easily for a pulsed Xe lamp was found to be 2:1 [25]. Another interesting finding reported from this study, is that the MIE decreases when the sample is exposed to several flashes. This was also reported in previous studies [11].

Moreover, experiments have also been conducted to decide which configuration is best for a laser pulse. Using a 1:2 weight ratio of as-prepared SWCNTs (APSWCNTs) to ferrocene, proved to require the least MIE to ignite the sample [33]. Here, "as-prepared" SWCNT means that the nanotubes have not undergone purification.

Another interesting aspect of the studies investigating the most efficient weight ratio, is that the MIEs are also reported. For a pulsed LED, the MIE was found to be $266\,\mathrm{mJ\,cm^{-2}}$ [36]. Meanwhile, for the Xe pulsed light, the MIE was shown to be $64.3\,\mathrm{mJ\,cm^{-2}}$ [25]. Additionally, Trewartha et al. observed a MIE of 110 mJ to ignite the 1:2 sample using a laser with a wavelength 1064 nm at a laser spot size of 4 mm. The MIE for a pulsed laser with the mentioned wavelength is calculated in Eq. 2.

$$\text{MIE per area} = \frac{110\,\mathrm{mJ}}{\pi \cdot 0.25 \cdot (4\,\mathrm{mm})^2} = 875\,\mathrm{mJ\,cm^{-2}} \tag{2}$$

Conclusively, different light source pulses do have different MIEs. Table 1 is included to give an overview of the previous experiments investigating ignition of samples of CNTs and ferrocene, using different light sources.

Table 1: Experimental results of igniting CNT using a Xe lamp, pulsed LED, and pulsed laser.

Pulsed light source	MIE	CNTs:ferrocene
Xe flash	$64.3\,\mathrm{mJ\,cm^{-2}}$ [25]	2:1 (MWCNT)
LED	$266\,\mathrm{mJ\,cm^{-2}}$ [36]	4:1 and 2:1 (MWCNT)
Laser	$875\,\mathrm{mJ\,cm^{-2}}$ [33]	1:2 (APSWCNT)

It has been shown in earlier studies that the ignition process using a light flash and a laser differs [33]. The reaction rate for the laser initiation of the combustion was found to be shorter compared to the regular flash unit. For the case of a laser, the initiation created a reaction close to an explosion, while for a flash, the reaction created a surface propagated deflagration.

In addition to this, the speed of which the energy is delivered also plays an important role. For a shorter pulse duration, it would require lower luminous energy to ignite the CNTs, compared to a longer pulse duration. It has been suggested that this phenomenon occurs due to the differences in time scales between energy transfer and dissipation [10]. This was also later backed up in 2014 [4]. In this experiment, they used a Xe camera flash, and it was also reported that the samples of SWCNT had the lowest MIE for a pulse duration of 120 µs.

Another phenomenon regarding the duration of which the luminous energy is transferred to the MWCNTs/ferrocene sample, is that the easiest sample to ignite depends on the luminous duration. For a continuous Xe lamp, it was found that the sample linked with the smallest MIE, was using a weight ratio of 1:3 [38]. On the other hand, for a pulsed Xe lamp, the MIE with the smallest value was found to occur at a weight ratio of 2:1 [25]. Therefore, the type of light duration also must be considered, when comparing the results to previous studies.

Furthermore, the choice between the sample with lowest MIE and the one with highest photo ignition temperature has to be made. As mentioned and shown previously, the weight ratio linked with the lowest MIE is two parts CNT to one part ferrocene, for a pulsed Xe lamp [25]. On the other hand, the weight ratio producing the highest temperature when exposed to a sufficiently powerful flash, is a ratio of 1:2 for MWCNT/ferrocene [33].

2.2 Xenon lamps

There are several possible light sources for igniting CNTs, but there are only some that are suitable for this type of application. Earlier there has been successful ignition using a Xe camera flash [25]. The most promising effect of using such a lamp, is the high luminous energy. As mentioned in Ch. 1.3, experiments have been conducted using LEDs and LDs, but it was concluded that both light sources delivered an insufficient amount of luminous energy for the intended setup.

Xe lamps consists of an anode, a cathode and a trigger coil, and are filled with pressurized Xe gas. When voltage is applied to the trigger coil, and thereafter the anode, the ionized gas emits white light for a short period of time. Ideally, a light source only emitting light close to UV wavelength would be used. This is due to the ignition threshold for CNTs and ferrocene reduces with reducing wavelength, as seen in Fig. 1.

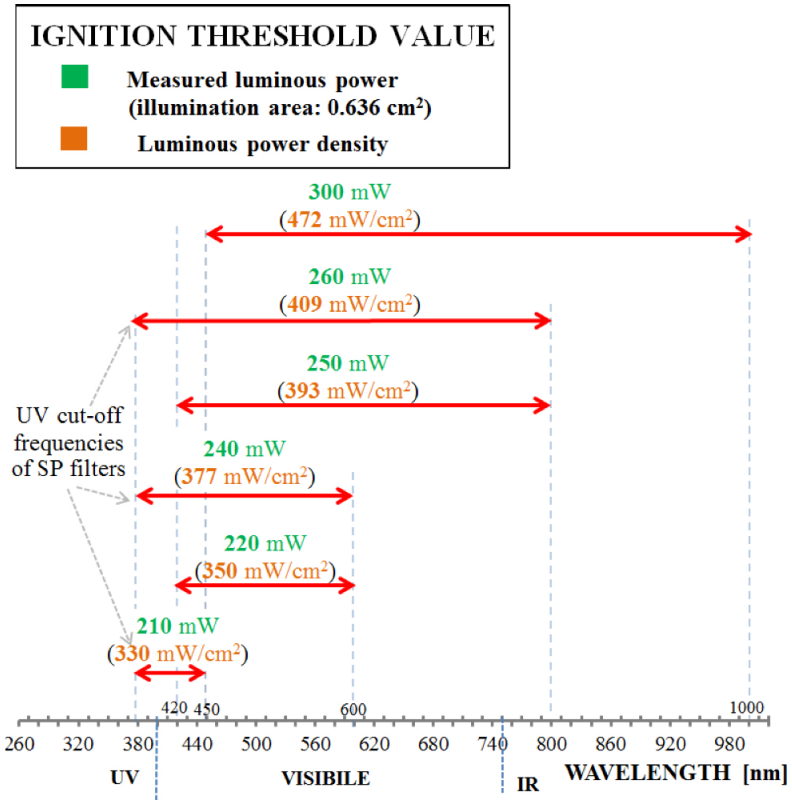

Figure 1: Ignition threshold for different wavelengths [38].

However, since no other available light source offer this kind of advantage, Xe flash tubes would still be the focus of this thesis.

To ignite CNTs, it would be preferable to focus the light into a singular point. This may not be applicable to combustion within a chamber, but it would be important to show a proof of concept. Light sources such as Xe lamps and LEDs emits incoherent light, different from a laser's coherent light [22]. This is also the reason why it is possible to focus the light from a laser into a singular point, but impossible using other light sources. The light emitted from a laser is a beam of photons that have the same frequency. Consequently, the light will not spread or diffuse. On the other

hand, the photons in incoherent light have different frequencies and are simultaneously oscillating in different directions.

Therefore, the light from a Xe flash could not be focused to a point smaller than the emitting surface. This is a disadvantage compared to for example a laser diode. A smaller beam would contain more energy per area, something that would be beneficial for the purpose of igniting the sample.

2.3 Driver

There are some certain specifications for the flash to be able to ignite CNTs. As mentioned, a short pulse is preferable, since this would require less energy delivered compared to longer pulse. To deliver such pulses, a driver able to generate pulses with a duration as low as possible is desirable. A typical flash circuit is illustrated in Fig. 2.

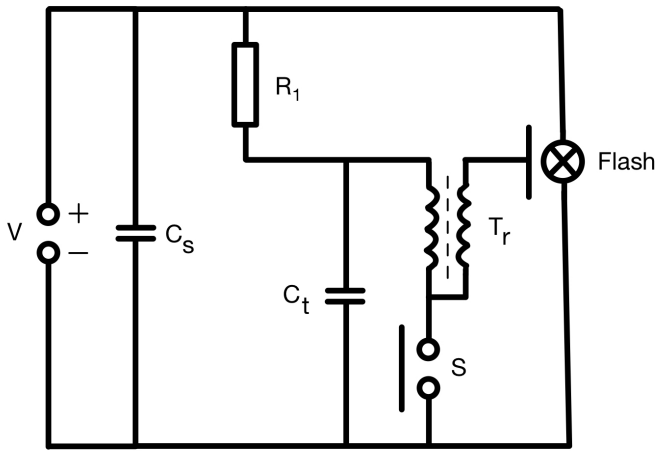

Figure 2: A typical flash circuit.

The procedure of flashing the Xe lamp is as follows [30]. Firstly, the capacitor, C_s, stores the electrical energy from the constant voltage supply, V, in an electrical field. The capacitor consists of two plates, one positive and one negative, separated by an insulting material. Both sides stores respectively positive and negative charge, but no electric charge can flow through, due to the insulation. After a given amount of time, the plates holds their maximum amount of charge. If the capacitor is then connected to a load, charge can flow from the positive to the negative side. Therefore, the capacitor now works as a source of electrical energy.

Afterwards, when C_s is fully charged and no more charge can flow through that loop of the circuit,

the charge flows through R_1 and the smaller trigger capacitor, C_t. This capacitor will receive a smaller voltage supply compared to C_s due to the resistor R_1.

As previously, no charge will flow through the loop containing C_t when it is fully charged. The next step is to close the switch S, such that charge can flow through the trigger coil T_r. C_t acts as a voltage supply, and the voltage is transformed from low voltage up to several kV using the coil. The pulse goes to the external envelope of the flash tube and in turn causes the gas within the Xe flash tube to ionize.

Finally, due to the ionized gases within the flash, the lamp is able to conduct electrical energy. Therefore, current flows from C_s to the flash. Hence, the flash is triggered. The flash tube keeps converting electrical energy to luminous energy for as long as the voltage that ionizes the gases is sufficiently high in order to conduct electrical energy.

2.4 Combustion and chamber physics

For these experiments, a static combustion chamber will be used. In contradiction to a common ICE, there is no piston moving within the chamber. Therefore, the combustion occurs at constant volume.

There are several physic phenomena happening in a combustion chamber. Mixing of gases, ignition of the said mixture, in addition to flame propagation, are all processes taking place during a short period of time.

The gases are injected through tubes going into the chamber. For these experiments, air and methane will be used in order to create a flammable mixture. To have a good understandable measurement of the weight ratio of both air and methane in an enclosure, the air-to-fuel ratio (AFR) is used [28]. This is defined in Eq. 2.

$$\text{AFR} = \frac{\text{Mass of air}}{\text{Mass of fuel}} \tag{3}$$

For example, an AFR equal to 1 is equivalent to the chamber containing the same mass of air and fuel. As the fuel needs a given amount of air in order to have a complete combustion, which is the stoichiometric air requirement, different masses of air and fuel is needed to fulfill this criteria. The fuel-air equivalence ratio is then the ratio between the stoichiometric AFR, from here on noted as AFR_{st}, and the AFR, as shown in Eq. 4.

$$\phi = \frac{\text{AFR}_{\text{st}}}{\text{AFR}} \tag{4}$$

From here on, the fuel-air equivalence ratio, ϕ, is shortened to the equivalence ratio. The air-fuel equivalence ratio is defined similarly in Eq. 5.

$$\lambda = \frac{\mathrm{AFR}}{\mathrm{AFR_{st}}} = \frac{1}{\phi} \tag{5}$$

In contradiction to the AFR, filling the chamber with air and methane such that ϕ is equal to 1, would yield a complete combustion. Since AFR equal to $\mathrm{AFR_{st}}$ gives ϕ equal to 1, this would be the stoichiometric equivalence ratio. Eq. 6 gives the chemical equation for stoichiometric combustion of methane and air.

$$\mathrm{CH_4} + 2\,\mathrm{O_2} + 2\,(3.76)\,\mathrm{N_2} \longrightarrow \mathrm{CO_2} + 2\,\mathrm{H_2O} + 2\,(3.76)\,\mathrm{N_2} \tag{6}$$

However, it could be desirable to run combustion engines on other equivalence ratios than the stoichiometric. If the AFR is adjusted to be larger than $\mathrm{AFR_{st}}$, the engine is said to be running lean. On the other hand, if the AFR is larger than $\mathrm{AFR_{st}}$, the ICE is running rich. Normally, spark ignition (SI) engines operates using equivalence ratios between 0.9 and 1.2 [28].

Due to high velocities within the combustion chamber, being generated by filling of the gases, turbulence will be present. In addition to the filling, a spinning fan is situated at the bottom of the chamber. Therefore, most of the flow in the enclosure is turbulent. This means that no combustion process will be equal, due to random fluctuations in motion for the particles involved. Furthermore turbulence enhances mixing, heat transfer, combustion rates and evaporation. Moreover, as turbulence is increasing, these parameters also increase.

Another physical phenomenon taking place within the static combustion chamber is swirl, which is generated by the fan. Similar to the turbulence, it also increases the mixing of the gases. In dynamic combustion chambers, swirl can be generated designing the valve ports, piston face or intake manifold [27]. However, since this is a static combustion chamber, with a gas inlet normal to the chamber wall, swirl will not be noticeably generated by injection of the gases.

After the ϕ is set to the desired value, and the gases are thoroughly mixed and pressurized within the combustion chamber, ignition can take place. Examples of different types of ignition is SI, compression ignition (CI) and photo ignition. The spark plug in a SI engine delivers between 30 and 50 mJ, where most of the energy is lost due to heat transfer [26].

The MIE required for igniting an air-methane mixture depends on several factors, such as for example pressure, temperature and equivalence ratio. As the pressure and temperature increases, the MIE decreases [13]. Additionally, the MIE is at its lowest when the equivalence ratio is slightly rich for an air-methane mixture [15]. The effect is especially noticeable at initial pressures lower

than 5 bar and temperature up to 30 °C, which is approximately the operating conditions for the experiments conducted in this thesis. Therefore, increasing the initial pressure in the combustion chamber, will make the MIE significantly decrease. The effects of change in pressure and temperature on MIE for an air-methane mixture at ϕ=1.0 are shown in Fig. 3.

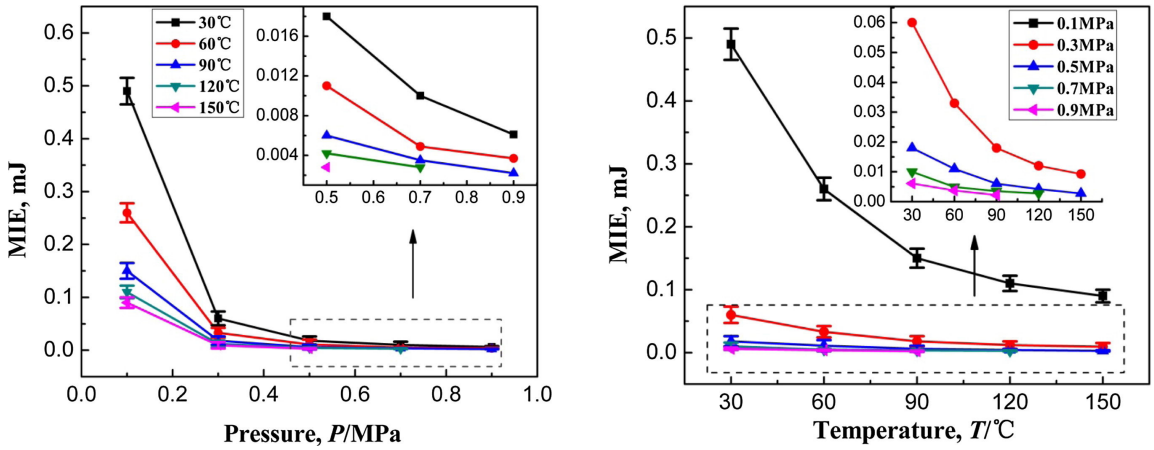

(a) Effect of pressure on MIE [13].

(b) Effect of temperature on MIE [13].

Figure 3: Effect of pressure and temperature on MIE for an air-methane mixture at ϕ=1.0.

Even though a sufficient amount of energy is delivered to the air-methane mixture, the unsuccessful ignition could still occur. One source for this error, is quenching of the flame. This happens due to heat transfer to the walls within the combustion chamber, which in turn reduces the flame front temperature [14]. Eventually, this leads to the flame being quenched.

As ignition of the air-methane mixture is successful and the combustion process begins, it is normal to divide this into three regions. The first one is the ignition and flame development. Here, the ignition and combustion process starts, but almost no increase in pressure is present. This is due to the flame being relatively small at the start of the combustion, which in turn leads to poor heating of the surroundings. Hence, the pressure within the chamber also remains low. If a slightly rich mixture is present next to the ignition point, the flame speed becomes faster and therefore a better combustion occurs [26]. Another word for this stage would be the ignition delay, the time from the ignition to a noticeable increase in pressure due to combustion. A typical pressure curve with the combustion processes is shown in Fig. 4.

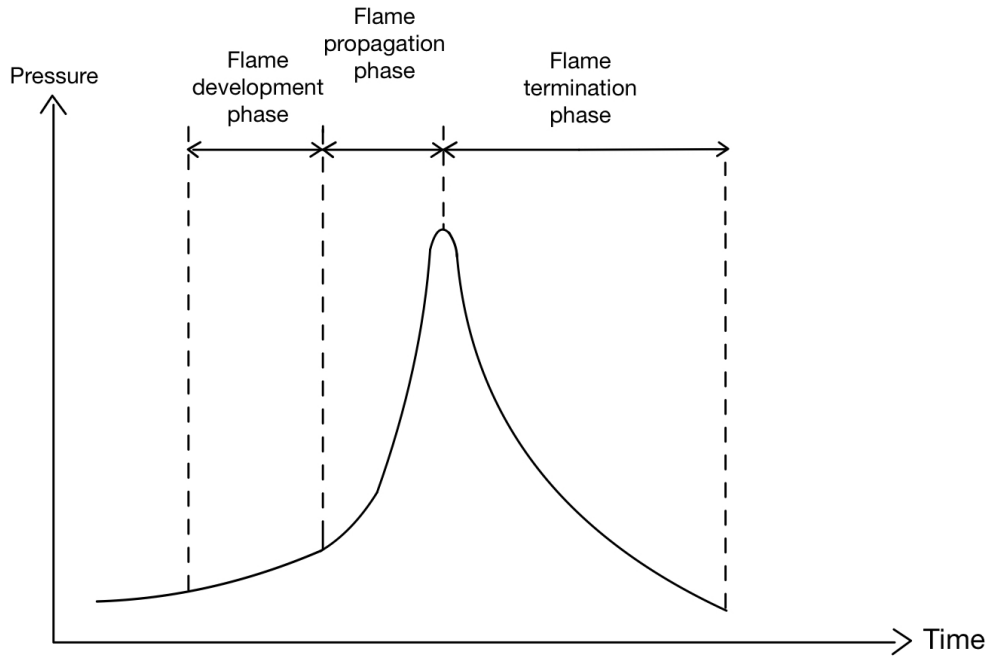

Figure 4: A typical pressure development and combustion processes for a static combustion chamber.

After approximately 5-10% of the mixture within the chamber has been burned, the combustion moves over to the next stage, namely the flame propagation phase. Here, the flame front moves quickly through the chamber, due to increased temperature and turbulence created in the first phase. As the flame propagates throughout the chamber, the already burnt mixture is hotter than the gases on the other side of the flame front. Since the entire mixture is approximately at the same pressure, the density of the burnt mixture increases. In turn, this leads to higher pressure and therefore higher temperature within the chamber. As a result, the flame is moving through an environment with progressively increasing temperature and pressure. Hence, the chemical reaction time decreases, leading to an increase of the flame speed [26].

Lastly, when 90-95% of the mass of methane and air have been combusted and the flame front has reached close to the walls of the chamber, the combustion process moves over to the next stage. Namely, the flame termination phase. Since the gases here is close to the wall, the turbulence of the remaining mixture drops due to the shear stress and the no-slip condition [26]. Additionally, the walls of the chamber acts like heat sinks conducting heat, causing the temperature to drop.

Therefore, the chemical reaction rate reduces, which leads to the flame terminating at a slow rate.

2.5 Photo ignition of air-fuel mixtures

As mentioned, photo ignition of air-fuel mixtures have been demonstrated previously. One of the studies conducted these experiments using a homogeneous mixture of air and ethylene [5]. It was shown that the photo ignition gave a quasi-homogeneous ignition of the mixture. Carlucci et al. on the other hand have shown the effect of photo ignition for fuels such as methane, hydrogen and liquefied petroleum gas (LPG) [8, 9]. For each of the aforementioned fuels, the photo ignition exhibits higher peak pressures, shorter ignition delays and higher fuel burning rates. Additionally, the result of using CNTs as a method for ignition in an internal combustion engine, is a system which requires 67 times lower MIE, compared to an original spark plug [1].

In particular, since the experiments in this paper is conducted using an air-methane mixture, the paper presented by Carlucci et al. in 2015 is especially interesting [8]. The graph shows increasing peak pressure for increasing equivalence ratios, while simultaneously decreasing the ignition delay. Note that the authors has used λ instead of ϕ. Experiments were conducted for equivalence ratios from 0.5 to 1, and the results are shown in Fig. 5.

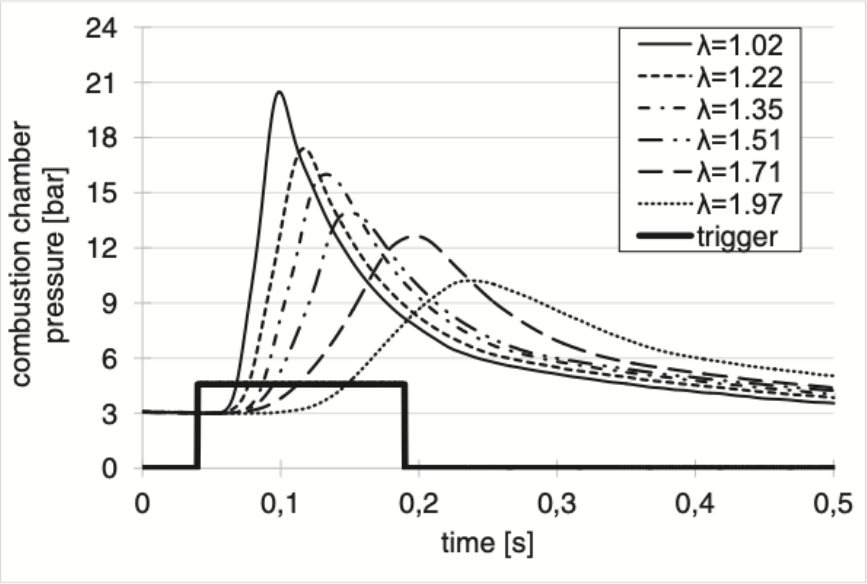

Figure 5: Photo ignition pressure developments for a range of ϕ at p=3 bar [8].

3 Methodology

3.1 Light sources

Several Xe light sources will be used in this project, including different linear and one round flash lamps. A combination of two linear lamps will be used to investigate the effect of the connecting multiple lamps together. For the lamps to be used in a series, two of the L-4040's are used, due to its geometry making them relatively easy to connect. Additionally, a camera flash will be tested to investigate if an out-of-the-box lamp will deliver a sufficient amount of luminous energy. The key features of the different lamps are given in Table 2.

Table 2: Key features for Xe lamps used for this project.

Manufacturer	Model	Type	Max energy	Dimensions
Xenonflashtubes	FT-40R	Round	100 J	39 mm x 9 mm (Flash diameter x Tube diameter)
Xenonflashtubes	L-4040	Linear	50 J	40 mm x 4 mm (Length x Diameter)
Xenonflashtubes	L-4040Q	Linear	150 J	40 mm x 4 mm (Length x Diameter)
Godox	AD600BM	Camera flash	600 J	220 mm x 125 mm x 245 mm (Height x Width x Length)

3.2 Experimental setup

3.2.1 Combustion chamber

As previously mentioned, the goal of this project is to ignite CNTs dispersed within the combustion chamber, using a light source situated outside of the chamber. In order to do so, a static combustion chamber with the possibility of injecting both gases and nanoparticles, combined with sensors for measuring pressure and temperature is needed. Sufficient strength of the chamber is also important to withstand the rapid pressure and temperature increases. Additionally, optical access to the chamber is important to be able to transfer energy from a light source outside to the CNTs within the chamber. Lastly, in order to investigate the effect of the photo ignition on the combustion, a spark plug is needed to compare the regular spark ignition to the mentioned photo ignition. An illustration of the combustion chamber and its parts are shown in Fig. 6, while an image of the experimental rig is shown in Appendix A.1.

A performance report is included in Appendix A.2, in order to show how the combustions using SI varies for experiments with the same initial conditions. Additionally, it is also shown how the combustion parameters differs when the equivalence ratio, ϕ, is changed.

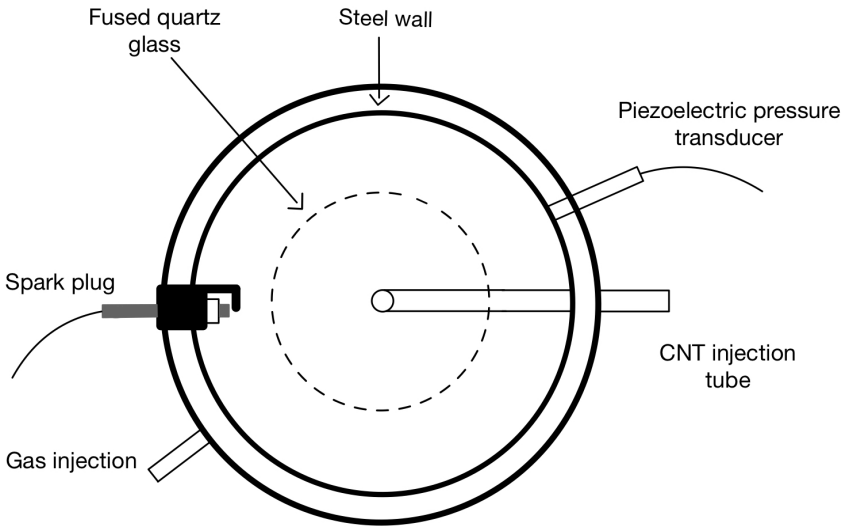

Figure 6: Combustion chamber used for ignition of CNTs.

The piezoelectric pressure transducer used for this experimental setup is a Kistler 6052C, which samples the pressure measurements at a frequency of 10 kHz, with a sensitivity of $20.8\,\mathrm{pC\,bar^{-1}}$.

Methane and synthetic air are used in order to replicate the environment within a conventional ICE. Synthetic air is used in order to avoid having unwanted elements within the injected air, since this would affect the chemical reactions. The method for filling the gases into the chamber is to set a desired synthetic air pressure and the desired equivalence ratio. Therefore, it is difficult to set the initial pressure of the air-methane mixture to exactly 1, 2, 3 and 4 bar. Hence, due to the amount of methane being small compared to the amount of synthetic air, the chamber pressures after filling will be a bit higher than the synthetic air pressure. Note that the pressures mentioned in this thesis, is the pressure value above the absolute pressure.

In addition to this, the CNTs are injected using a certain amount of nitrogen. A simplified illustration of the injector is shown in Fig. 7. The amount of nitrogen injected is small compared to the molar mass of methane and synthetic air within the combustion chamber, in order to negligibly affect the mixed gases. In order to use a fixed amount of nitrogen, a manual valve is included before the holding chamber. It is closed before injection of the particles into the combustion chamber. Consequently, the amount of nitrogen injected into the combustion chamber only depends on the pressure of the supply.

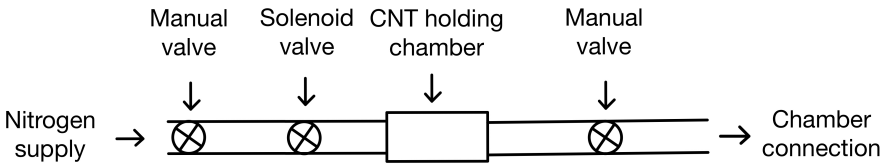

Figure 7: System for injecting samples of CNTs and ferrocene into the combustion chamber.

The manual valve after the holding chamber is opened before opening the solenoid valve. The pressure within the CNT holding chamber and the tube from the manual valve to the holding chamber is atmospheric. Since the pressure within the combustion chamber is higher than the atmospheric pressure, due to injection of methane and synthetic air, the CNTs stays within the holding chamber. It is not until the solenoid valve opens, and the nitrogen with higher pressure than the combustion chamber reaches the holding chamber, that the CNTs are injected.

A possibility of adjusting the time interval between the solenoid valve opening and the flash being triggered is present. It is important to investigate when to trigger the light source, in order to ignite the CNTs dispersed within the chamber. Therefore, some measurements have to be taken to calculate the time from opening of the solenoid valve, to the flash being triggered. To investigate this matter, a camera with a high frame speed is used to be able to analyze the injection process of the CNTs.

3.2.2 Filming injection of CNTs

In order to decide which operating conditions that most likely could ignite CNTs within the chamber, it is desirable to investigate videos of injection of CNTs into the chamber through different tubes and for different pressures. By doing so, it is possible to understand which tube and pressure gives most CNTs in front of the window of the chamber at a given time.

The camera being used is a Photron Fastcam NOVA S6. This camera is capable of filming the injection at frame speeds up to 6400 frames per second (fps), while maintaining a resolution of 1024 x 1024, for investigating the presence of CNTs. Due to the combustion chamber being dark and containing no light sources, a light source is placed on the opposite side of the chamber for the camera, as seen in Fig. 8. A diffuser is mounted between the chamber and the light source in order for the camera to have uniform background lighting. If the diffuser would not have been in place, a large point source would appear in the videos, due to light only coming from a bulb within the lamp.

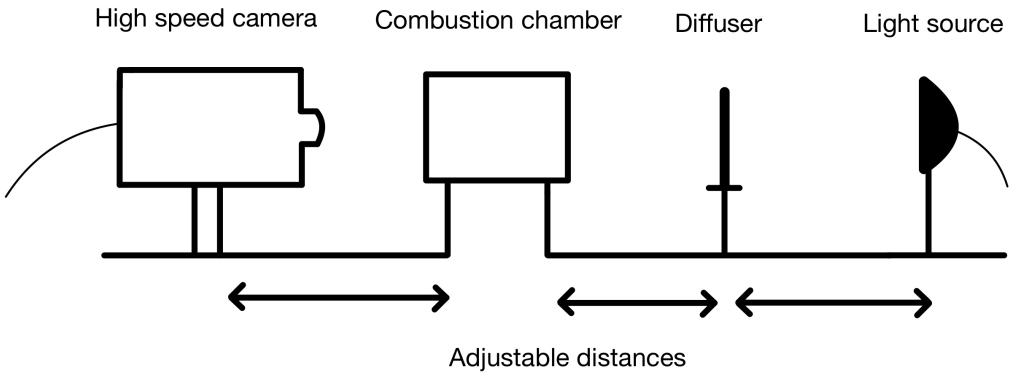

Figure 8: Experimental setup for filming the injection of CNTs.

The distances between the camera, combustion chamber, diffuser and light source are all adjustable. These adjustments, in addition to the settings on the camera, are important in order to optimize the quality of the videos.

3.2.3 Measurement of fluence

To investigate the different Xe lamps capability of igniting the MWCNTs/ferrocene samples, a method for generating and measuring the most possible luminous energy from the camera flash and the standalone Xe lamps, has been developed. An energy and power meter equipped with a pyroelectric sensor are obtained in order to conduct these experiments. The working principle of the pyroelectric sensor is close to that of the capacitor, presented in Ch. 2.3. Such a sensor consists of two electrodes, where one of them has a black coating, which is the one exposed to the luminous energy [24].

The heat from the radiation is absorbed by the black coating and thereafter transported into a ferroelectric crystal material situated between the electrodes. Hence, a pyroelectric voltage is generated due to charge being transported from one electrode to another, which in turn can be transformed into an electrical signal. Therefore, it is possible to measure the luminous energy which is absorbed by the pyroelectric sensor.

The physical property being measured is the fluence, which is the optical energy per unit area [23]. Similar to the optical intensity, the fluence is position dependent. Therefore, the fluence is highest along the beam axis. For the experiments conducted in this thesis, the fluence is assumed constant over the entire sensor.

Before conducting experiments to ignite CNTs using a flash, it is desirable to compare the luminous

energy delivered from available light sources to the MIE found in literature, shown in Table 1. In order to do so, the pyroelectric sensor is used to measure the fluence emitted from the flash. The method of experimentally conducting these measurements is to flash the light source at a given distance from the sensor, for a given number of times. This is done in order to ensure that the results do not vary notable for each flash. Thereafter, the distance between the light source and the pyroelectric sensor is changed, to obtain an understanding of how the luminous energy varies with distance from the light source. An experimental setup for testing the Xe flash tubes connected to the circuit board, is illustrated in Fig. 9.

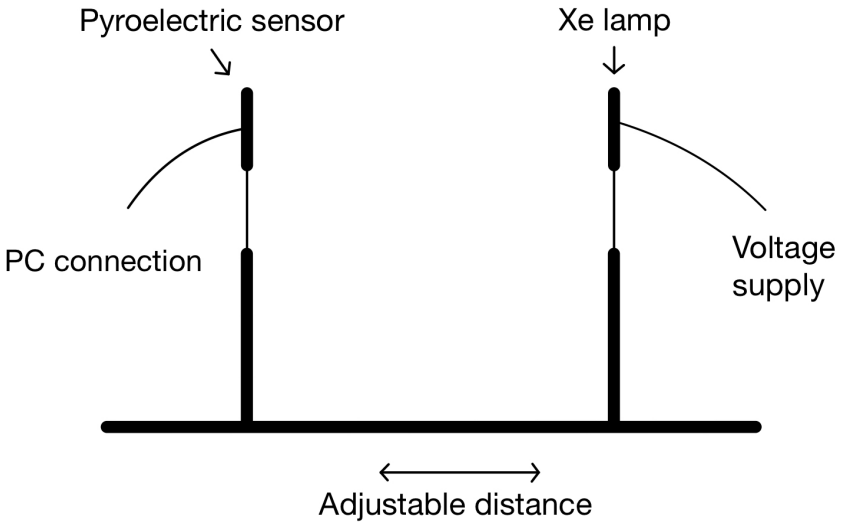

Figure 9: Experimental setup for fluence measurements for Xe lamps.

For these experiments, the energy and power meter being used is a Thorlabs PM103, while the pyroelectric sensor is a Thorlabs ES145C. The sensor has an energy range of 500 µJ to 2 J. Additionally, the diameter of the sensor area is 45 mm.

In addition to the smaller Xe flash tubes, a setup for testing the camera flash is made. Since the bulb of the camera flash is not symmetric, tests were conducted to measure the fluence at different angles of the flash tube as well. These setups are shown in Appendix C. The luminous energy measured at the front of the flash tube, which is the z-direction in Fig. 28a, is from here on not noted with the specific direction.

3.2.4 CNTs and ferrocene

There are especially two stages to consider regarding the CNTs and ferrocene, namely the mixing and the filling.

In order to mix the samples of CNTs and ferrocene thoroughly, two methods for mixing the two particles are used. A random amount of MWCNTs from Nanografi with 96% purity and a diameter between 8 and 18 nm is filled into a container. The sample is then weighted using a Sartorius Entris analytical balance scale, which has a precision of 0.1 mg. For a given weight ratio of CNTs and ferrocene, the correct amount for the decided ratio of ferrocene, from Sigma Aldrich, is filled into the same container. Thereafter, the container is shaken in order to enhance mixing of the two different substances.

Meanwhile for the second sample, a pestle and mortar are used. Firstly, the procedure is equal to the other method for mixing. The CNTs are put into a container and weighed. Thereafter, the nanoparticles of carbon is put into the mortar, while the correct amount of ferrocene is put into the container and weighed. Finally, the ferrocene is placed into the mortar. Then the pestle is used to ensure good mixing, before the mixed sample is transferred back into the closed container.

As no relatively accurate scales have been available continuously at the lab, the method for separating the amount of the samples has been to use a spoon. The accuracy for each experiment will therefore not be exact. An experiment was conducted in order to find the standard error and average weight for each spoon, seen in Table 3.

Table 3: Uncertainty in sample weight.

No. of experiments	Average	Min	Max	Standard deviation	Standard error
16	12.18 mg	8.20 mg	16.60 mg	2.41 mg	0.60 mg (4.95 %)

Since the standard error is relatively low, less than 5 % than the average weight of one spoon, the measuring of the amounts of the sample used is sufficiently accurate. As from here on, the amount of one quarter, one, two and three spoons will be given respectively as 3 mg, 12 mg, 24 mg and 36 mg.

3.2.5 Ignition outside of the combustion chamber

The ignition experiments outside of the combustion chamber will be conducted in order to gain a better understanding of how the available light sources performs considering ignition of CNTs. However, the sample should be dispersed quasi-homogeneously within the combustion chamber. Therefore, ignition of a pile of CNTs and ferrocene would not give a complete understanding of

the MIE for the sample within the chamber. On the other hand, this experiment should give an indication of which light source to use and at which distances ignition could be expected.

In order to investigate the ignition characteristics of the CNT mixture, experiments outside of the combustion chamber were conducted. The setup for these experiments is shown in Fig. 10. Firstly, a sample of CNTs and ferrocene is placed onto the Petri dish, with a light source placed above the sample. Thereafter, a Xe flash is triggered in order to ignite the mixture. If ignition is not achieved, the sample of CNTs and ferrocene is changed with a new fresh sample, and the distance between the Petri dish and the Xe lamp is reduced by a small increment. The procedure is repeated until ignition is achieved for all the different samples of CNTs and ferrocene.

As mentioned earlier, previous studies have found that the MIE reduces for several consecutive flashes. Therefore, it is important to replace a flashed non-ignited sample with a new, fresh sample.

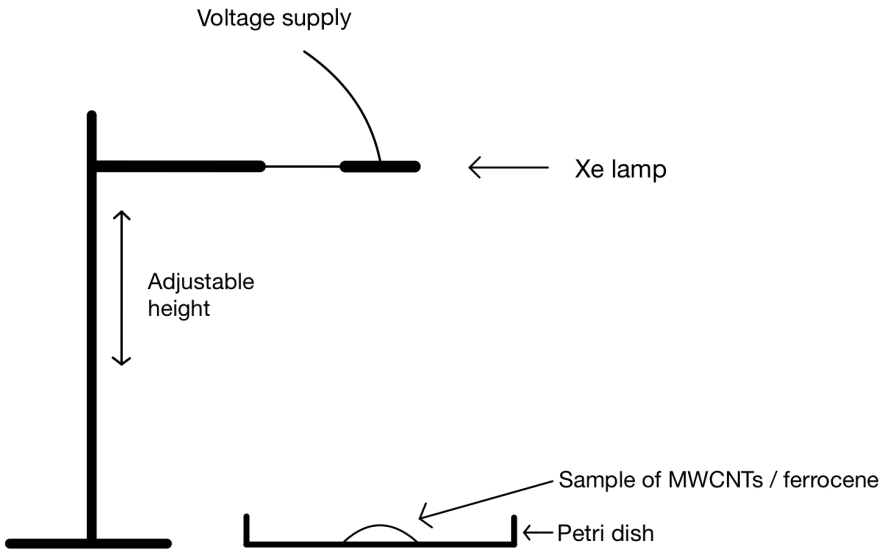

Figure 10: Experimental setup for ignition of CNTs outside combustion chamber.

3.2.6 Ignition within the combustion chamber

In the introduction, it was stated that the goal of this project is to ignite mixture of CNTs and ferrocene within a combustion chamber using a flash of light. The experimental setup for this particular experiment is illustrated in Fig. 11.

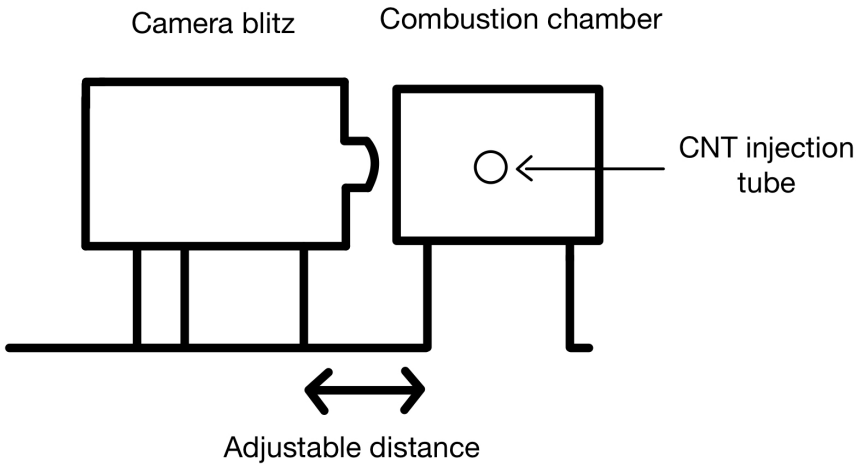

Figure 11: Experimental setup for ignition of CNTs within combustion chamber.

The sample containing CNTs is transported into the combustion chamber using nitrogen and a tube, before being exposed to a Xe flash. The distance between the chamber and the light source is adjustable, in order to optimize the ignition process. A greater distance means less luminous energy delivered into the chamber and to the CNTs. Therefore, a maximum distance for ignition would give the MIE for dispersed CNTs within the combustion chamber. In order to keep the camera flash in an upright position, a simple tool was designed, shown in Fig. 12.

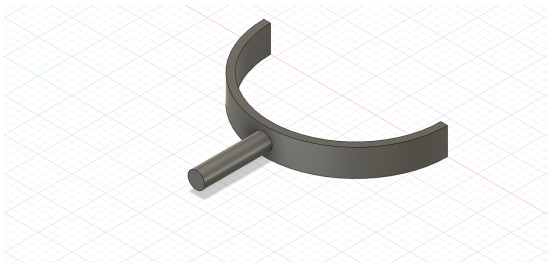

Figure 12: Mount for the camera flash.

Similarly to the injection of particles, the combustion is also an interesting process to film. However, since it is uncertain if the Photron Fastcam tolerates the high luminous energy being released from the flash tubes, another camera will be used. This is a Promon U750, capable of maintaining a resolution of 800 x 600 at 511 fps while filming.

3.3 Driver

As mentioned in 2.3, a short flash combined with a high luminous energy is desired. Except for the camera flash, all Xe lamps needs an external voltage input. A driver from Xenonflashtubes is used. It is capable of delivering up to 260 J, depending on the capacitors mounted on the circuit board. The driver requires two capacitors, and for this project, two pairs of capacitors are tested. One pair delivers a total of 98 J, while the other pair gives an output of 260 J. The capacitors with highest capacitance were only used for conducting experiments with the most powerful linear Xe flash.

A BK Precision Bench Power supply 1687B is used for the required 12 V voltage supply for the circuit board. The output voltage delivered from the driver, ranging from 250 V to 700 V, is adjustable using a knob mounted on board. As the adjustment of the knob is not very precise, only three settings will be used; lowest possible (low), highest possible (high) and in the middle between the lowest and highest (middle). However, it is not known how the voltage output varies between these knob positions.

The circuit board is designed such that a voltage drop closes the switch, S, illustrated in Fig. 2. Hence, the method for triggering the flash is to apply a constant 5 V signal to the circuit, and thereafter cut the said signal. In order to apply such a signal, a square pulse from an Aim-TTi TGP110 Pulse Generator is used.

At the start of the project, only one driver was available for use. Later on, two more similar drivers were acquired, since it is undesirable to solder one pair of capacitors and thereafter detach, and reattach a new pair. This is done in order to avoid problems with soldering and possibly damaging the circuit board, in addition to have a backup.

A security aspect for this driver is that the voltage going through the circuit could be up to 6 kV. Therefore, it would not be safe to have a standalone circuit board. To overcome this problem, a secure enclosure needed to be made, in order to ensure a safe operation. Images of the box that was 3D-printed are shown in Fig. 13.

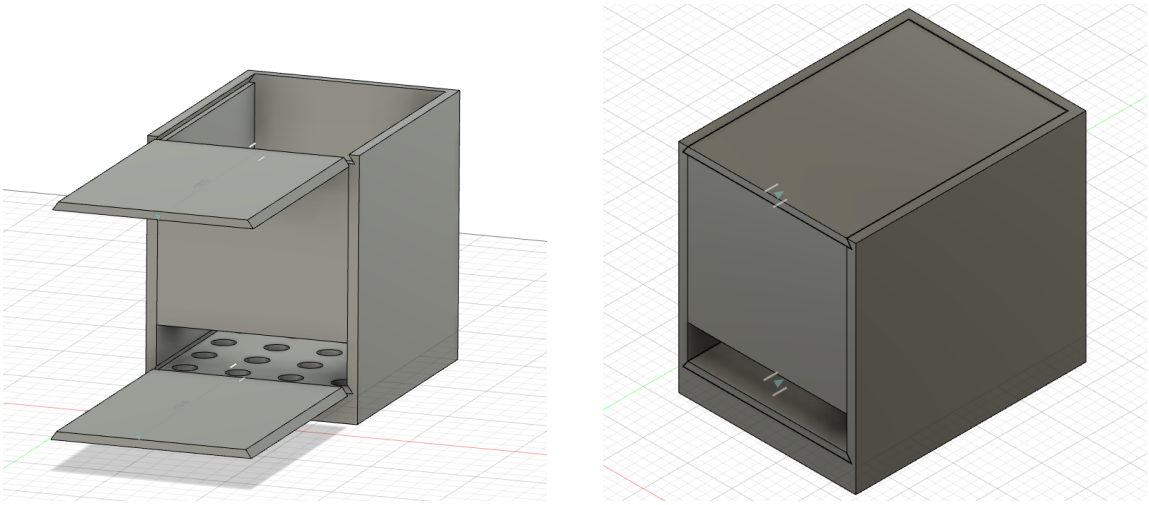

(a) Circuit box open. **(b)** Circuit box closed.

Figure 13: Circuit board box.

The holes in the bottom of the box is made in order to easily screw the box onto the rest of the Thorlabs equipment in the lab. The slider at the bottom is then fitted into place, to ensure no conducting of current from the circuit board to the screws. The slit is included for two specific reasons, where one of them is to have an opening for the wires to exit the box. Additionally, the slit ensures for operation of the knob, which controls the voltage output. The top slider is there to prevent the circuit board falling out of the enclosure during transportation.

3.4 OACIC mount

Timewise, the final objective of this thesis, was to switch from the static combustion chamber to the OACIC, shown in Appendix B. As will be discussed in Ch. 4.3.2, time constraints made the switch not happen. Nevertheless, a system for mounting the Xe lamps connected to the circuit board onto the OACIC has been made and is ready to use for further experiments.

A method for mounting the circuit box and the Xe lamp onto the OACIC was needed. A 3D-printed tool is shown in Fig. 14.

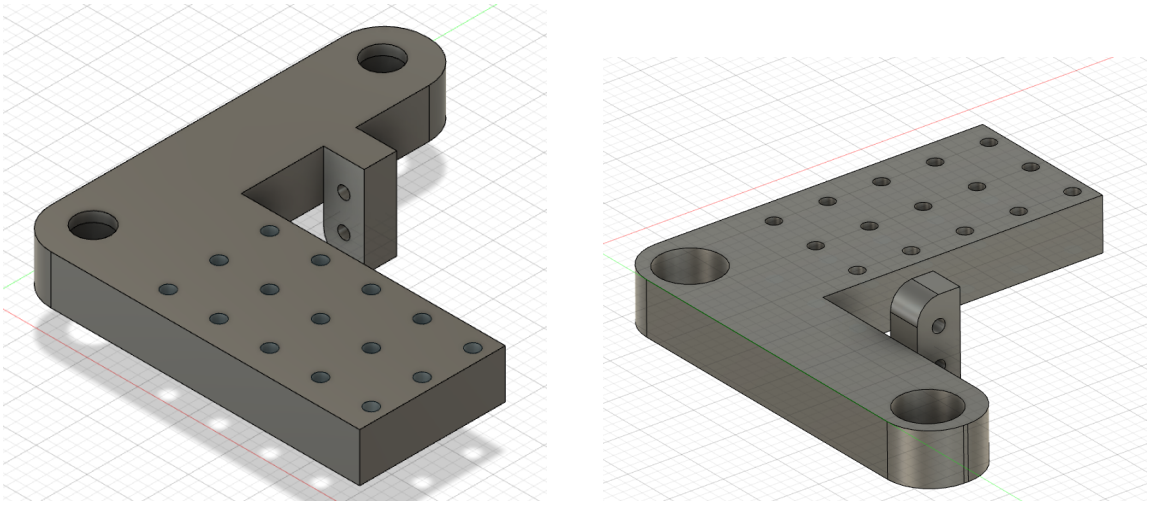

(a) Mount for OACIC seen from the top.

(b) Mount for OACIC seen from the bottom.

Figure 14: Mount for OACIC.

The two larger holes are used to place the tool onto two bolts and screws situated at the top of the OACIC. Meanwhile, the board containing more holes is used to easily mount the circuit board onto the engine. This is necessary, due to the rocking motion of the OACIC. If the board would not have been mounted on the engine, but only the Xe lamp, a possible damaging of the wires going from the board and to the lamps could occur. This would in turn lead to a short circuit. Therefore, it was essential to connect the box to the engine. The knob was designed in order to have a mount for placing the light source in front of the optical access of the engine.

When the mount for the OACIC was finished, all that was left was to create a tool for mounting the Xe lamp in front of the optical access to the engine. This needed to be connected to the engine mount, in addition to fixing the position of the Xe lamp during operation. The finished designs are shown in Fig. 15.

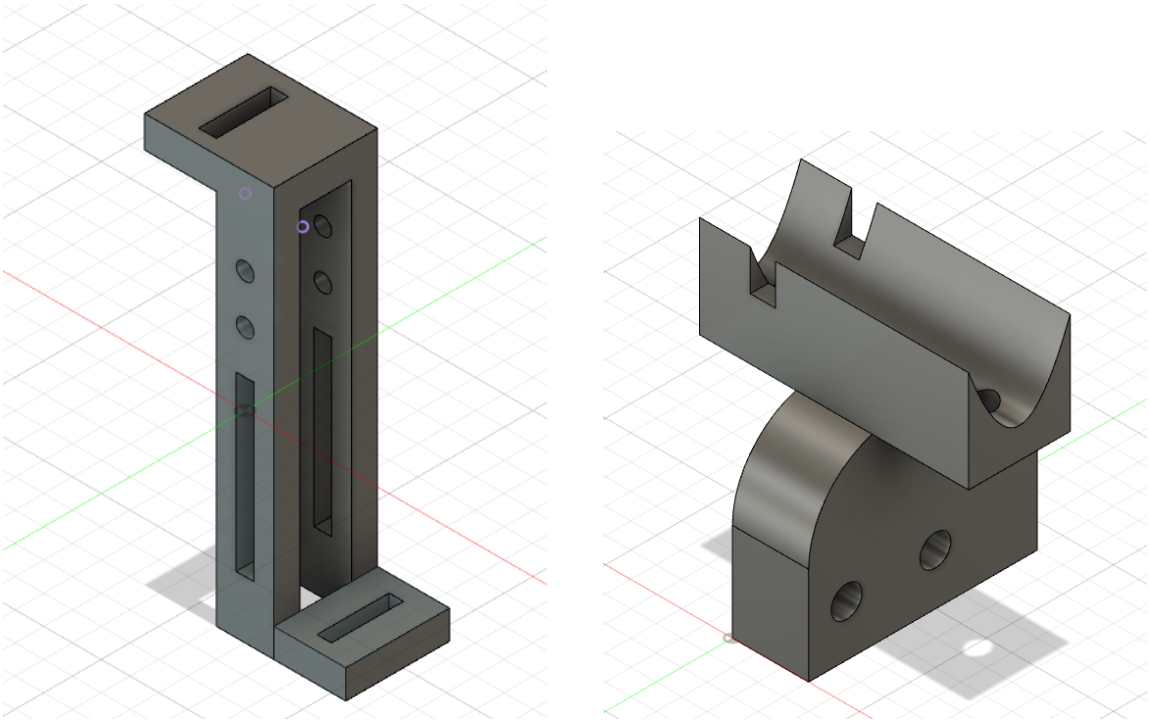

(a) Mount for the reflector. **(b)** Reflector for the Xe lamp.

Figure 15: Tools designed to mount Xe lamp onto the OACIC.

The holes in the sides of the mount in Fig. 15a were made such that a screw could be placed through this tool and the main mount in Fig. 14. Hence, this device would be fixed during operation. Meanwhile, the slits on the sides were made to fix the Xe lamp, using the reflector in Fig. 15b. The slit seen on top of Fig. 15a, was designed for the tool to be used on different Thorlabs equipment, since the slit fits the screws used. On the contrary, the slit at the bottom was designed in order to keep the wires from the Xe lamp in place.

Lastly, the reflector in Fig. 15b was made for the linear Xe lamps. This equipment mounts on the mount shown in Fig. 15a using the standard Thorlabs screws. Two holes are situated in the reflector area, in order to fix the Xe lamp using its wires. The slit on top of the reflector area is made to fit the trigger coil wire from the Xe lamps. The inside of the area was at first coated with aluminium foil, in order to have the possibility of investigating the advantage of having a reflector. No such tool was made for the round Xe lamp and the camera flash, due to their already high output energy.

3.5 Health, safety and environment

Since the nanoparticles exposes a health hazard, as reported in [31], health, safety and environment (HSE) assessment had to be conducted for the handling of the CNTs. The samples are always transported in closed containers outside of the glove box, available at the lab. Additionally, masks with a high efficiency particulate air (HEPA) filter, safety glasses and gloves were used when refilling the samples onto the glass plate and the basket. These experimental setups are shown in Fig. 19 and will be presented in Ch. 4.3.2.

There was also conducted a HSE assessment for the operation of the combustion chamber. Operators of the rig had to wear safety glasses, and stay behind a wall made of acrylic glass, separating them and the combustion chamber for each ignition attempt.

4 Results and discussion

4.1 Xe lamp tests

As shown in Table 2, several Xe lamps were available in this project in order to investigate a suitable light source for photo ignition. The method for comparing the different lamps was shown in Fig. 9. The results of the measurements using the pyroelectric sensor for the different configurations for the light sources are shown in Fig. 16.

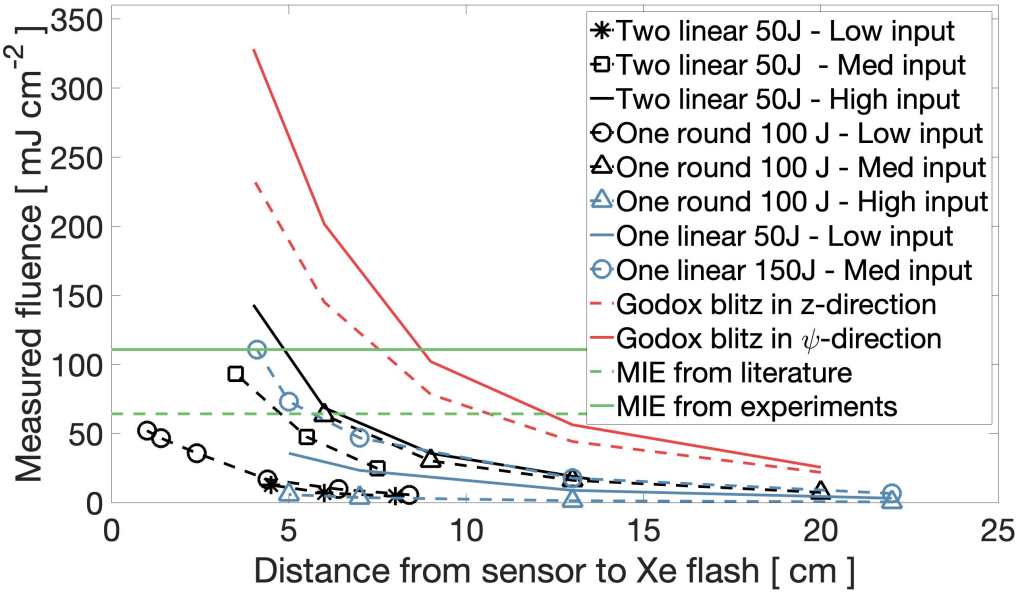

Figure 16: Comparison of different Xe flashes.

The MIE from the lab is obtained using the experimental data from the conducted experiments reported in Ch. 4.3. Both of the minimum MIE's shown in the graph are obtained using samples of CNTs and ferrocene with weight ratio of 2:1.

It is observable that several different light sources delivers a sufficient amount of luminous energy in order to ignite the sample containing CNTs and ferrocene within the chamber. However, it is the camera flash that shows most promising results, with a predicted maximum ignition distance of approximately 9 cm.

As discussed in Ch. 3.2.3, the camera flash is not symmetric, unlike the other light sources. It is observable that it is the top and bottom of the flash tube, which emits most fluence. This makes sense, due to there being a larger area of the flash tube at these positions. A closer investigation

of the fluence as a function at the different angles of the flash tube is given in Appendix C. It is not given in detail in this section, due to the only possible method for mounting the camera flash in front of the optical access of the combustion chamber, is as shown in Fig. 12.

The two linear 50 J lamps connected in series also showed encouraging results. Unfortunately, the two flash tubes broke after a short period of time being triggered. This incident also led to the circuit board becoming damaged, likely due to a short circuit following the Xe lamps being destroyed. After some troubleshooting, it was concluded that the circuit board was beyond an easy repair. Adding to this blow for the project, no new circuit board did arrive until two months later. Therefore, a long period of time did pass by without a light source, before the camera flash arrived six weeks before the end of the project.

4.2 Injection

It was important to decide which pressure to use for the injection of the CNTs and at which time after opening the solenoid valve it was desired to trigger the flash. In addition to these methods for varying the injection, the amount of the sample of CNTs and ferrocene could also be varied. Injection tubes with different diameters were also tested in this experiment, in order to get a complete understanding of the injection process. The setup used for conducting these experiments, was presented in Fig. 8.

A MATLAB script, shown in Appendix D, was used to calculate the frame containing most particles in front of the camera. The method for this calculation is to detect the particles as different grayscales, which has different values for the amount, or intensity, of light. The sample, which is black, will create a high value pixel. Hence, it is possible to decide which frame and therefore at which exact time, it should be most easily to ignite the mixture. As residuals could appear on the quartz glass between experiments, the average values of the first 5 frames for each video is used as a reference for the respective calculation, in order to detect the injected sample. Therefore, the calculation is independent of the base state of the quartz glass for each experiment.

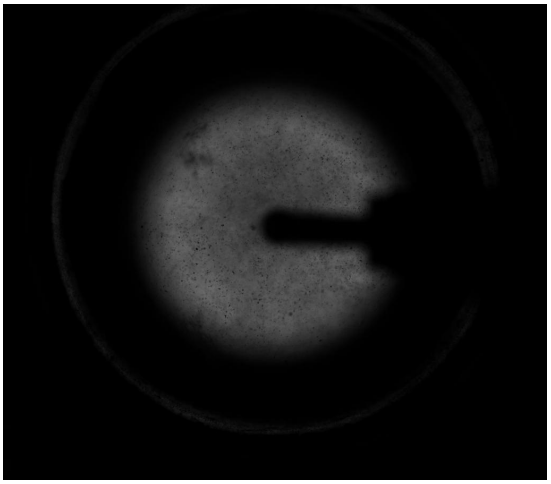

(a) Injection test using sample weight of 12 mg at N_2 equal to 2 bar using medium tube.

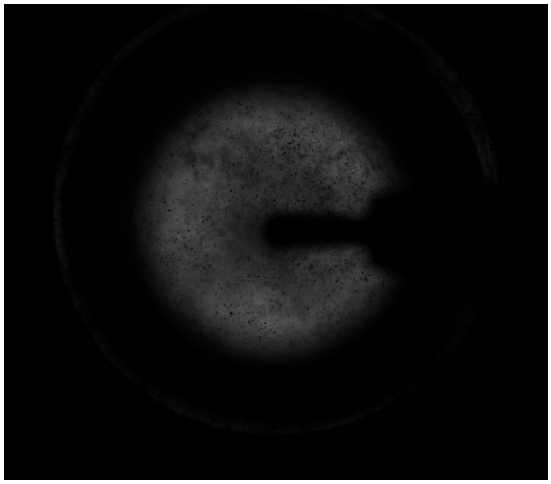

(b) Injection test using sample weight of 24 mg at N_2 equal to 2 bar using medium tube.

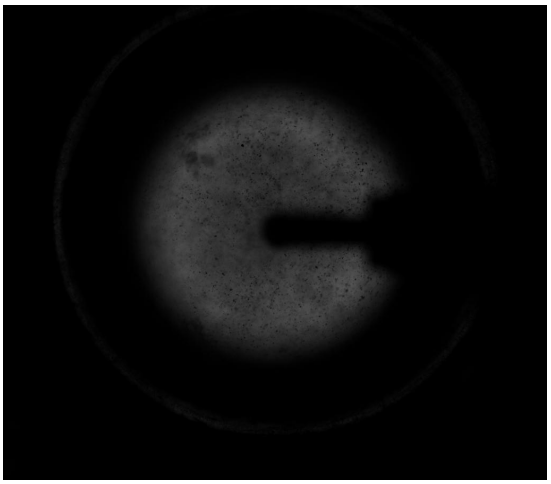

(c) Injection test using sample weight of 36 mg CNT at N_2 equal to 2 bar using medium tube.

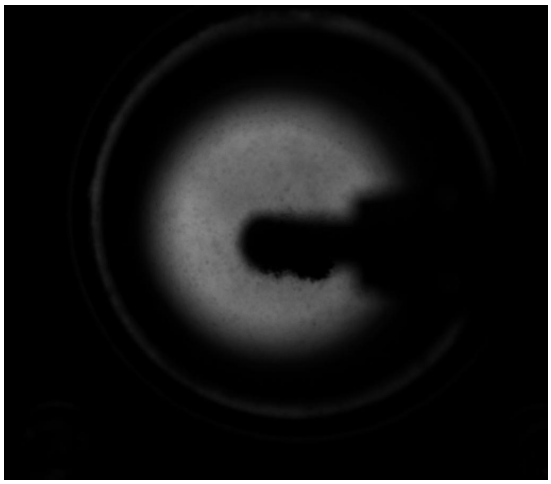

(d) Injection test using sample weight of 24 mg at N_2 equal to 4 bar using large tube.

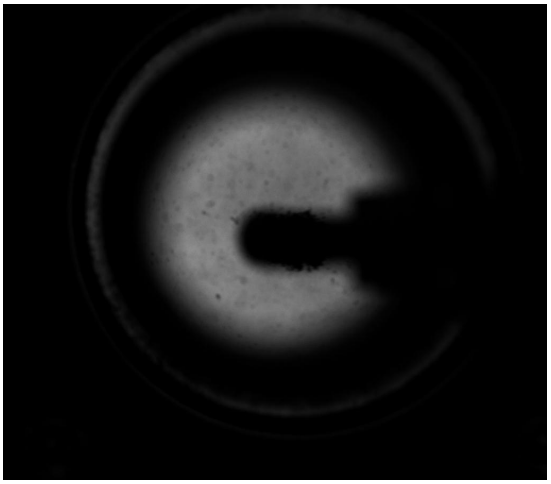

(e) Injection test using sample weight of 24 mg at N_2 equal to 2 bar using large tube.

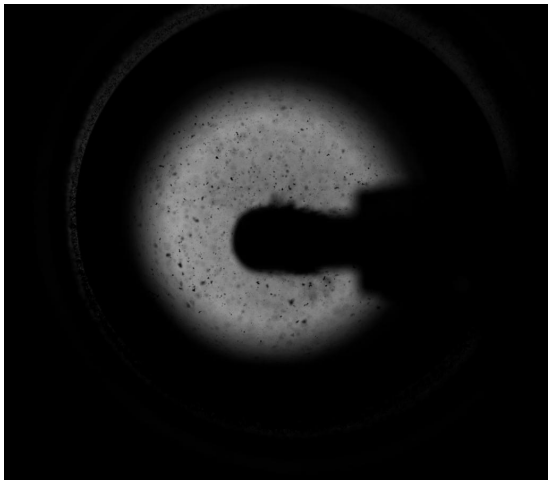

(f) Injection test using sample weight of 12 mg at N_2 equal to 2 bar using large tube.

Figure 17: A selection of the experiments where the effect of varying the tube diameter, in addition to the amount of CNTs and ferrocene, on dispersion.

Looking at the images shown in Fig. 17, it is evident that the medium tube showed great potential for igniting the injected sample of CNTs and ferrocene. The image with largest amount of particles in front of the quartz glass can be argued to be Fig. 17b and Fig. 17c. However, it is clear that the large tube, where the injections are seen in Fig. 17d to 17f, does not produce as much of the dispersed samples in front of the quartz glass, when compared to the injections using the medium tubes.

One reason for this occurrence could be that more of the sample is sticking to the quartz glass after the injection using the large tube. The explanation for this phenomenon could derive from the different diameter of the tubes leading to the tube outlet velocities being unlike. A bigger diameter should give a smaller outlet velocity, which could lead to the sample not hitting the quartz glass hard enough to bounce back into the chamber. This would in turn lead to a larger residual of the sample stuck on the glass, which is unfavorable for having a quasi-homogeneous dispersed sample within the combustion chamber.

Increasing the amount of the sample of CNTs and ferrocene from 12 mg to 24 mg and finally 36 mg does have an effect on the injection as well. The increase of particles in front of the quartz glass is seen from Fig. 17a to Fig. 17c. Whereas the increase from 12 mg to 24 mg is easy to spot, the difference between 24 mg and 36 mg is harder to observe. It seems to be that 24 mg of the sample produces a more favorable ignition possibility compared to 36 mg. Therefore, it was concluded that 24 mg of the sample, combined with a medium tube and an inlet pressure of 2 bar, should provide

the highest probability of igniting the mixture within the chamber.

It is important to note that the pressures given in Fig. 17 is the pressure above the absolute pressure within the combustion chamber. Through the entire results section, all pressures are defined as pressures above the absolute pressures.

4.3 Ignition

4.3.1 Outside of the combustion chamber

The experiments regarding ignition of CNTs and ferrocene conducted outside of the combustion chamber was performed in order to gain an understanding of which distances successful ignition could be expected. The setup for these experiments was illustrated in Fig. 10. The outcome of this investigation is shown in Table 4 for the round Xe lamp and Table 5 for the camera flash.

Table 4: Experimental results of igniting CNT using a round Xe lamp.

CNTs:ferrocene	Maximum ignition distance	MIE
1:4	3.9 cm	115.5 mJ cm^{-2}
1:3	3.7 cm	117.5 mJ cm^{-2}
1:2	3.9 cm	115.5 mJ cm^{-2}
1:1	4.1 cm	110.8 mJ cm^{-2}
2:1	4.1 cm	110.8 mJ cm^{-2}

Table 5: Experimental results of igniting CNT using a Xe camera flash.

CNTs:ferrocene	Maximum ignition distance	MIE
1:4	4.7 cm	233.6 mJ cm^{-2}
1:3	5.0 cm	222.7 mJ cm^{-2}
1:2	5.2 cm	217.9 mJ cm^{-2}
1:1	5.4 cm	201.1 mJ cm^{-2}
2:1	5.4 cm	201.1 mJ cm^{-2}

As seen in Fig. 16, the camera flash should be more powerful than the round Xe lamp. Therefore, the results obtained and shown in the two tables above are as expected. The camera flash manages to ignite the sample of CNTs and ferrocene at larger distances, compared to the round Xe flash. The quartz glass has a depth of 2.4 cm, so the round Xe flash is only capable of igniting a pile of CNTs and ferrocene 1.7 cm into the chamber, in order for the sample to be successfully ignited.

Alternatively, the camera flash has to be used. This light source is more powerful compared to all of the other tested in this project, but is only capable of igniting particles at a distance of 3.0 cm into the combustion chamber. In total, the combustion chamber is 20.5 cm, so the sample being dispersed throughout the chamber would be senseless, due to the particles further away from the glass would receive an insufficient amount of energy in order to be ignited. Conclusively, the sample should be focused towards the quartz glass.

As stated in Ch. 4.1, the camera flash should be expected to ignite the sample of CNTs and ferrocene at a distance of approximately 9 cm. However, it only manages to ignite the sample at a maximum of 5.4 cm. The MIE reported in literature is also lower compared to the lowest MIE obtained in these experiments, as seen in Fig. 16. An important thing to note, is that the fluence used for the MIE is the same fluence as for the entire sensor surface area. In hindsight, the sample of CNTs and ferrocene being of a smaller area compared to the sensor area should have been compensated. This would have taken into account that the energy being transferred to the sample, is not the same as to the pyroelectric sensor, due to having a smaller area. Therefore, it is reasonable that the MIE reported in these experiments are higher compared to the experiments reported in the literature [25].

An experiment was also conducted in order to investigate the effect of the different mixing methods of CNTs and ferrocene on the MIE, as mentioned in Ch. 3.2.4. The results from these experiments are shown in Table 6.

Table 6: Experimental results of comparing different methods for mixing CNTs and ferrocene.

CNTs:ferrocene	Maximum ignition distance for		MIE for	
	pestle and mortar sample	shaken sample	pestle and mortar sample	shaken sample
1:1	4.9 cm	5.4 cm	221.8 mJ cm^{-2}	201.1 mJ cm^{-2}
2:1	5.2 cm	5.4 cm	217.9 mJ cm^{-2}	201.1 mJ cm^{-2}

It is evident that different methods for mixing of the particles does have a say regarding the MIE for the samples. This could therefore be one source of error for the MIE, since the mixing of the particles could have been done differently in previous experiments. However, due to the shaken sample having the smallest MIE, this procedure will be used for future experiments as well.

On the other hand, this would not explain why the MIE of the round Xe flash and the camera flash differs. For example, the shape of the flash tube could affect the ignition process. One method to investigate this matter would be to have two flash tubes with equal maximum energy ratings, but different geometry. Hence, if experiments were conducted in order to find the maximum distance for successful ignition, and the distances for the two Xe lamps were unequal, the shape would have

to affect the MIE. Since such Xe lamps were not available during this project, this experiment could not be conducted.

As both the round Xe flash and camera flash uses similar methods for converting electrical energy to luminous energy, the values for the MIE in Table 4 and Table 5 should have been more similar. The shape of the flash tube could affect the ignition of the sample, as previously mentioned. Additionally, the shape could affect the fluence being measured by the pyroelectric sensor. As stated in Ch. 3.2.3, it is assumed a constant fluence over the entire sensor. However, the geometry of the two flash tubes could therefore affect the calculation of the fluence done by the measurement tools.

Nevertheless, the camera flash had been proven to be the light source which most easily ignited the sample of CNTs and ferrocene. Therefore, this would also be used for further experiments.

4.3.2 Within the combustion chamber

A chronological summary of the ignition tests within the combustion chamber is shown in Tab 7. All tests were done with the camera flash placed as close to the quartz glass as possible. This is just a selection of the experiments conducted, in order to show how scientific progress was made.

The term sample placement denotes where the sample of CNTs and ferrocene are placed, before being exposed to the flash. For example, "Tube" is equivalent to the sample being put into the holding chamber and injected using a gas, using the system for injection shown in Fig. 7. Parameters such as "Basket" and "Glass plate" will be introduced more in detail later in this chapter. The injection pressure and gas refers to the system for injecting CNTs and ferrocene into the combustion chamber, shown in Fig. 7. Initially, nitrogen was used as the system gas, at a given pressure, which is the injection pressure. The air pressure is the pressure above the absolute pressure of the air filled into the combustion chamber, before the filling of the methane. Some experiments do not have listed a successful or unsuccessful photo ignition. These experiments were not conducted due to time constraints, but it is strongly suggested that they are executed for future studies.

Table 7: Chronological development of experiments within the combustion chamber. No value in photo ignition column refers to an experiment which was not conducted, but is strongly suggested to conduct in further experiments. Sample placements will be given in detail in this section.

No.	CNT: ferrocene	Mass of sample	Sample placement	Injection pressure	Injection gas	Air pressure	Flash delay	Fan	ϕ	Photo ignition
1	1:1	24 mg	Tube	2 bar	Nitrogen	2 bar	200 ms	On	1	No
2	1:1	24 mg	Tube	4 bar	Nitrogen	1 bar	690 ms	Off	1	No
3	2:1	24 mg	Tube	4 bar	Nitrogen	1 bar	200 ms	Off	1	No
4	2:1	24 mg	Tube	4 bar	Nitrogen	1 bar	150 ms	Off	1	No
5	2:1	24 mg	Tube	4 bar	Nitrogen	1 bar	100 ms	Off	1	No
6	2:1	24 mg	Tube	5.1 bar	Nitrogen	2 bar	100 ms	Off	1	No
7	2:1	24 mg	Tube	6.2 bar	Nitrogen	3 bar	100 ms	Off	1	No
8	2:1	24 mg	Chamber	6.2 bar	Nitrogen	3 bar	100 ms	Off	1	No
9	2:1	36 mg	Chamber	6.2 bar	Nitrogen	3 bar	100 ms	Off	1	No
10	1:2	36 mg	Basket (aluminium)	-	-	3 bar	100 ms	Off	1	No
11	1:2	36 mg	Basket (quartz filter)	-	-	3 bar	-	Off	1	No
12	1:2	36 mg	Glass plate	-	-	3 bar	-	Off	1	No
13	1:2	36 mg	Glass plate	-	-	3 bar	-	Off	1.2	No
14	1:2	36 mg	Glass plate	-	-	3 bar	-	Off	0.8	No
15	1:3	24 mg	Glass plate	-	-	4 bar	-	On	1	No
16	1:3	12 mg	Glass plate	-	-	4 bar	-	On	1	No
17	1:3	3 mg	Glass plate	-	-	4 bar	-	On	1	No
18	1:2	36 mg	Glass plate	5.5 bar	Synair	4 bar	100 ms	On	0.8	Yes
19	1:2	24 mg	Glass plate	5.5 bar	Synair	4 bar	100 ms	On	0.8	Yes
20	1:2	12 mg	Glass plate	5.5 bar	Synair	4 bar	100 ms	On	0.8	Yes
21	1:2	36 mg	Glass plate	5.5 bar	Synair	4 bar	100 ms	On	0.7	Yes
22	1:2	24 mg	Glass plate	5.5 bar	Synair	4 bar	100 ms	On	0.7	Yes
23	1:2	12 mg	Glass plate	5.5 bar	Synair	4 bar	100 ms	On	0.7	Yes
24	1:2	36 mg	Glass plate	4.5 bar	Synair	3 bar	100 ms	On	0.7	Yes
25	1:2	36 mg	Glass plate	3.5 bar	Synair	2 bar	100 ms	On	0.7	Yes
26	1:2	36 mg	Glass plate	2.5 bar	Synair	1 bar	100 ms	On	0.7	No
27	1:2	36 mg	Glass plate	4.5 bar	Synair	3 bar	100 ms	On	0.8	Yes
28	1:2	36 mg	Glass plate	3.5 bar	Synair	2 bar	100 ms	On	0.8	No
29	1:2	36 mg	Glass plate	2.5 bar	Synair	1 bar	100 ms	On	0.8	No
30	1:2	36 mg	Glass plate	5.5 bar	Synair	4 bar	100 ms	On	0.9	No
31	1:2	36 mg	Glass plate	4.5 bar	Synair	3 bar	100 ms	On	0.9	-
32	1:2	36 mg	Glass plate	3.5 bar	Synair	2 bar	100 ms	On	0.9	No
33	1:2	36 mg	Glass plate	2.5 bar	Synair	1 bar	100 ms	On	0.9	No
34	1:2	36 mg	Glass plate	5.5 bar	Synair	4 bar	100 ms	On	0.6	No
35	1:2	24 mg	Glass plate	4.5 bar	Synair	3 bar	100 ms	On	0.6	-
36	1:2	12 mg	Glass plate	3.5 bar	Synair	2 bar	100 ms	On	0.6	-
37	1:2	12 mg	Glass plate	2.5 bar	Synair	1 bar	100 ms	On	0.6	-
38	1:2	36 mg	Glass plate	5.5 bar	Nitrogen	4 bar	100 ms	On	0.8	Yes
39	1:2	36 mg	Glass plate	-	-	4 bar	-	On	0.8	-
40	1:2	24 mg	Tube	5.5 bar	Synair	4 bar	160 ms	On	0.8	No
41	2:1	24 mg	Tube	5.5 bar	Synair	4 bar	160 ms	Off	0.8	-

Experiment 1 for igniting CNTs within the combustion chamber, was done to investigate if the system was operating as desired. As seen in Table 7, the operating conditions for this experiment were not properly set. A chamber pressure higher than the injection pressure meant that the sample with CNTs would not be injected into the chamber. Additionally, the fan was also used for this experiment. This would increase the turbulence within the combustion chamber, which furthermore increases mixing within the chamber. By using the fan, the CNTs would become more dispersed, which is positive regarding the desired output of the experimental project. On the other hand, a quasi-homogeneously dispersed CNT sample would be harder to ignite, and therefore not desired in order to have a successful proof of concept. Hence, it was decided to not use the fan until a successful ignition of the CNTs within the chamber occurred. Due to the aforementioned unfortunate experimental configurations, no successful ignition was achieved.

Experiment 2 was conducted while the fan was turned off, increasing the nitrogen pressure to a higher level than the chamber pressure, combined with reducing the mentioned chamber pressure. Additionally, a higher ignition delay was randomly chosen, due to a desire of having as much particles in the chamber as possible. There was no evidence suggesting a successful photo ignition in this experiment.

Before going through with experiment 3, it was decided that a proper investigation of the ignition delay needed to be conducted. Earlier experiments, as seen in 4.2, have suggested that the amount of CNTs in front of the quartz glass varies greatly with time. Therefore, the camera was mounted onto the test rig once more, in order to investigate the injection process. The experimental configuration for the camera test was similar to experiment 2, listed in Table 7. Fig. 18 shows the results and development of this injection.

There are samples of CNTs stuck on the quartz glass before this experiment was conducted, which could be seen in Fig. 18a. After approximately 29 ms, samples of CNTs is showing in the video. This can be seen in Fig. 18b.

The same MATLAB script as used in Ch. 4.2, was used in order to investigate which flash delay would optimize the possibility for a successful photo ignition of the air-methane mixture. For this case, the situation occurs after 113 ms, shown in Fig. 18c.

Another interesting point for ignition of the CNTs occurs 205 ms after opening the solenoid valve, seen in Fig. 18d. Here, the velocity of the particles is smaller compared to the earlier stages. Nevertheless, a lot of particles are still seen in front of the quartz glass. Therefore, this is also an interesting timing for triggering the flash.

In experiment 3, the flash delay is set to 200 ms, in order to have a high possibility of igniting the sample within the combustion chamber. The rest of the operating conditions are kept equal to the conditions used for filming the injection. This is due to different operating conditions would yield

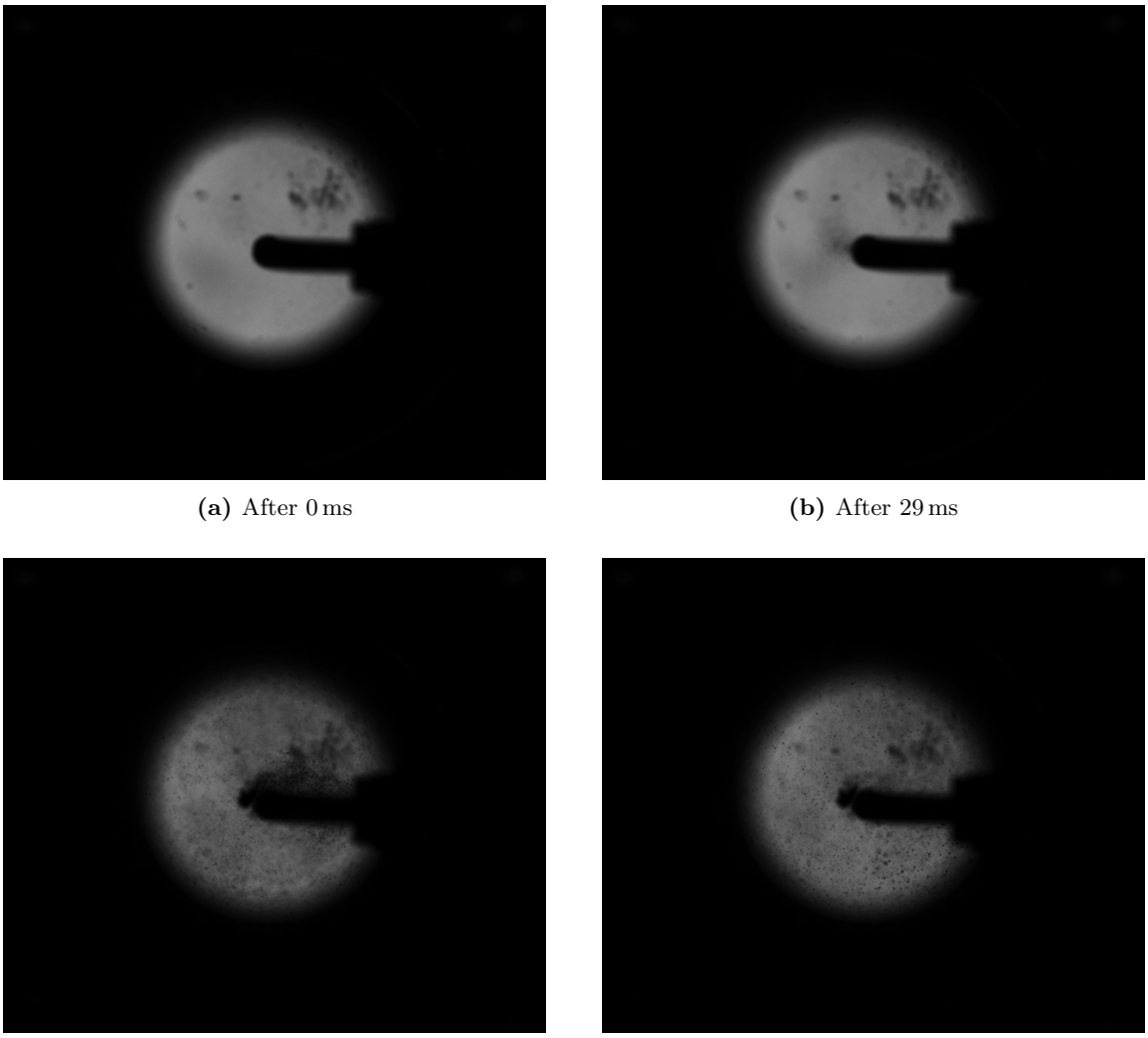

(a) After 0 ms

(b) After 29 ms

(c) After 113 ms

(d) After 205 ms

Figure 18: CNTs dispersed in front of quartz glass a given amount of time after opening of injection solenoid valve, using ϕ=1.0 and p=4 bar.

different flash delays. However, also for this experiment a successful ignition was detected.

Another experiment with the flash delay reduced to the mean of the two desired flash timings was conducted, shown in experiment 4. Unfortunately, no successful ignition was achieved.

After discarding the flash delay found by visual investigation, the calculated timing was used in experiment 5. The rest of the operating conditions was the same as used in the previous experiment. A residual, similar to the one seen in Fig. 18a, was spotted at the quartz glass before the triggering of the flash. No ignition of the air-methane mixture was achieved in this experiment, but the residual on the window appeared to have ignited during the flash. However, the energy released from the ignition of the particles could not have had the required energy for igniting the air-methane mixture. Therefore, the pressure were increased in experiments 6 and 7 in order to reduce the MIE for igniting the methane. Still no successful ignition of the mixture was achieved.

Having tried to ignite the air-methane mixture using photo ignition at air pressures up to 3 bar, different measures had to be considered in order to achieve a successful ignition. Since there was observed residual of ignited samples with carbon nanotubes and ferrocene, it was concluded that the camera flash delivered a required amount of energy into the chamber. From Fig. 16, it is observable that the energy from the camera flash increases exponentially when reducing the distance between the flash and the sensor. Therefore, it was desirable making sure that the particles within the chamber were as close as possible to the light source. Additionally, the weight ratio of CNTs and ferrocene was changed from 2:1 to 1:2, since this, as shown in Ch. 2.1, produces the highest flame temperature for the sample.

To test this hypothesis, a pile of nanoparticles was placed on the other side of the quartz glass for the camera flash. The configuration is shown in experiment 8 in Table 7. Using 24 mg of the sample, no flame was seen in the chamber. It was decided to increase the amount of nanoparticles to a sample weight of 36 mg, to fix this problem and in contrast to previous experiments, a flame was seen on the inside of the optical access. The flame produced a lot of smoke within the chamber. However, the air-methane mixture was not ignited, which was believed to be due to quenching.

In order to ensure less heat transfer to the chamber and therefore quenching, a basket filled with the sample and covered with aluminium foil, was placed next to the quartz glass within the combustion chamber. By doing so, the sample containing ferrocene and CNTs was placed at a fixed distance of approximately 3 cm from the light source. As seen in Fig. 16, at this specific distance, the energy from the camera flash should be more than powerful enough in order to ignite the sample within the chamber.

The use of the basket was partly successful, due to the nanoparticles being ignited in the basket. On the other hand, the burning pile did not spread out in the chamber and did not ignite the air-methane mixture. As the luminous energy from the camera flash did not reach the nanoparticles

at the bottom of the basket, a new configuration had to be made. It was decided to use a glass plate fixed in the middle of the optical access of the combustion chamber, such that the luminous energy and access to the rest of the chamber would be maximized. Additionally, the glass plate was covered with thermal tape, in order to reflect as much heat as possible into the chamber. Both of the setups for the basket and the glass plate, without the thermal tape, are shown in Fig. 19,

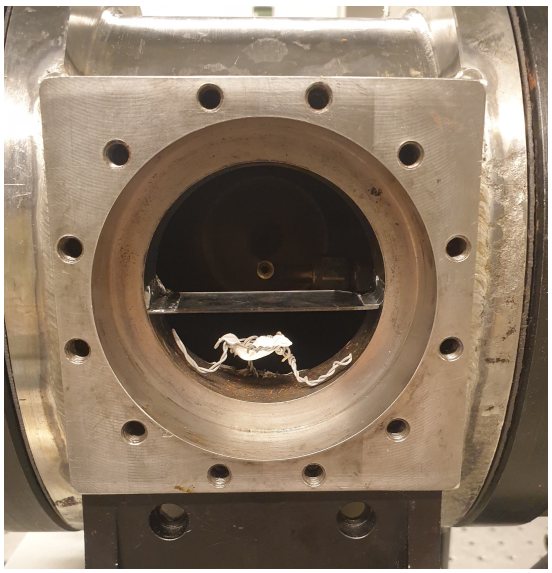

Figure 19: Experimental setup for both glass plate and basket.

After having made the setup using the glass plate, it was obtained successful ignition of the sample containing CNTs and ferrocene for each attempt. However, the air-methane mixture did not ignite. In experiments 12-14 in Table 7, three different equivalence ratios were tested, but neither ignited anything more than the sample. Hence, other procedures had to be considered.

As mentioned in Ch. 2.4, the ignition energy of the air-methane mixture reduces when increasing the initial pressure in the combustion chamber. Therefore, it was decided to increase the air pressure to 4 bar, in addition to changing the weight ratio to 1:3, due to a low MIE being reported in previous studies [38]. These researchers used a continuous Xe lamp, while in this case a pulsed Xe lamp is used. However, since Table 4 and 5 showed small variations in MIE for the different samples, it was considered something worth to investigate.

Experiment 15, using 24 mg of the sample, did not produce a successful combustion, but it did produce a flame. Since the basket setup gave an unsuccessful photo ignition for this amount, it was concluded that the glass rig was indeed a better option. Despite having improved the experimental rig, no combustion of the air-methane mixture occurred. The next two experiments were conducted

using smaller amounts of nanoparticles, all the way down to 3 mg, in order to investigate the effect of adjusting the amount of sample. Even though a flame occurred in each experiment, the sample did not ignite the air-methane mixture.

As the sample of CNTs and ferrocene stayed at the glass plate for the entire combustion of the particles, it was decided to attempt to spread the burning sample further into the chamber. In order to investigate this proposition, the nitrogen supply for injecting the particles into the chamber was used. Unlike previous experiments using this system for injection, shown in Fig. 7, no particles would be placed into the holding chamber. Therefore, only the gas used to inject the particles, was utilized to spread the sample situated on the glass plate.

In addition to including the nitrogen circuit into the experimental setup once more, it was chosen to substitute nitrogen with synthetic air flowing through the circuit. The reason for this change, was to compensate for the oxygen used in oxidation reactions with the CNTs and ferrocene, as stated in Eq. 1. Since the methane requires oxygen in order to release energy through chemical reactions, shown in Eq. 6, this change was considered necessary.

After adjusting the ϕ down to 0.8 in experiment 18, while simultaneously changing the circuit gas from nitrogen to synair and using the MWCNT:ferrocene sample with a weight ratio of 1:2, successful photo ignition was achieved, using a light source placed outside of the combustion chamber. The development of the ignition and combustion is shown in Fig. 20.

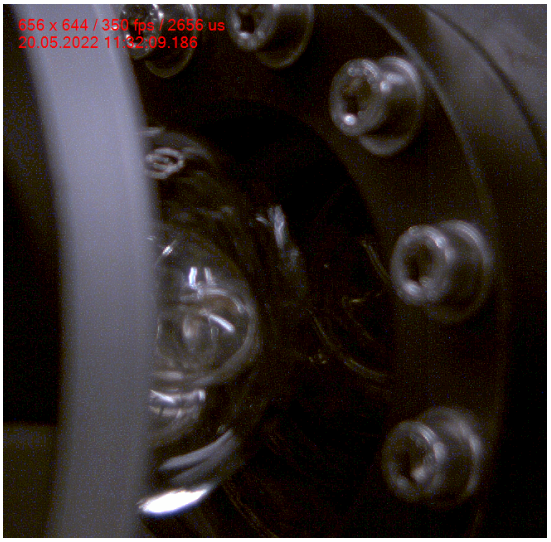

(a) Before trigger - 0 ms

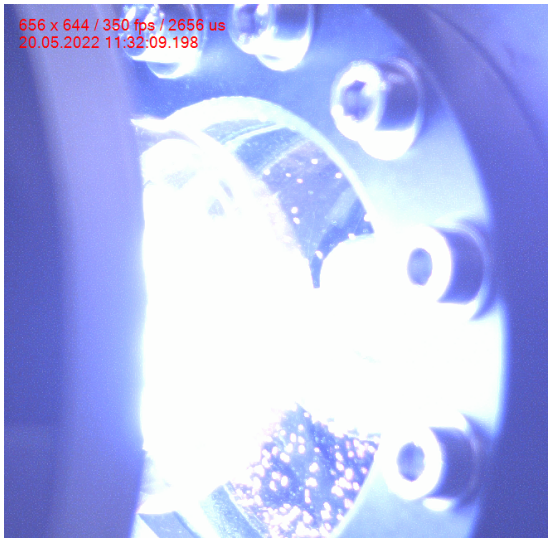

(b) Flash triggered - 3 ms

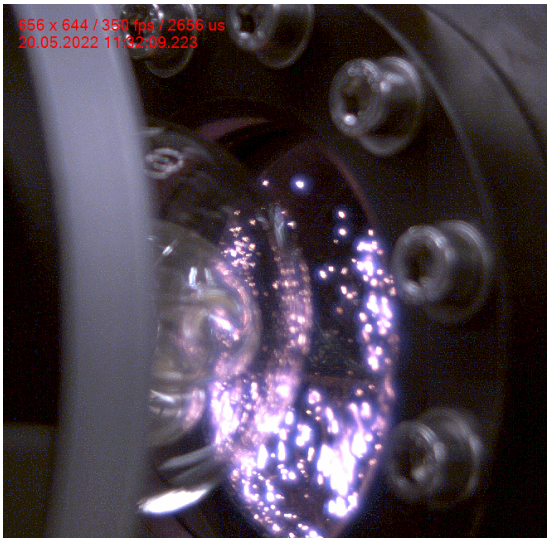

(c) After trigger - 37 ms

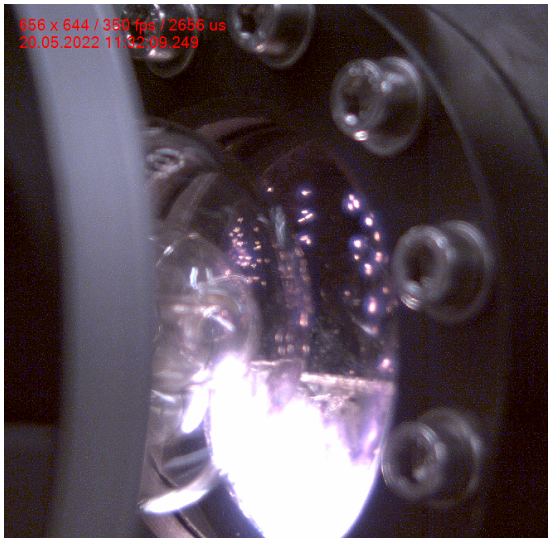

(d) Flame development phase - 63 ms

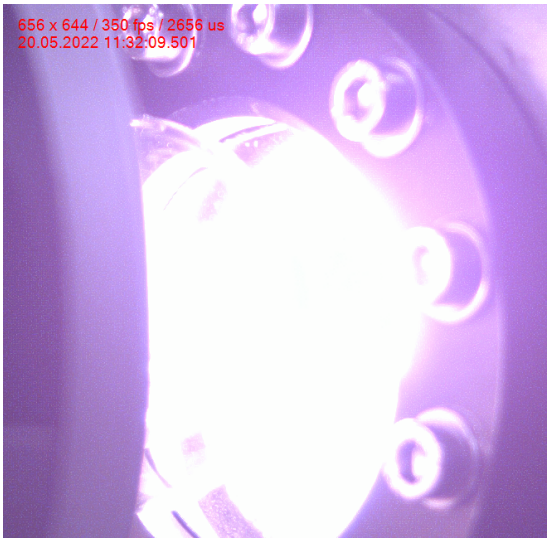

(e) Flame propagation phase - 315 ms

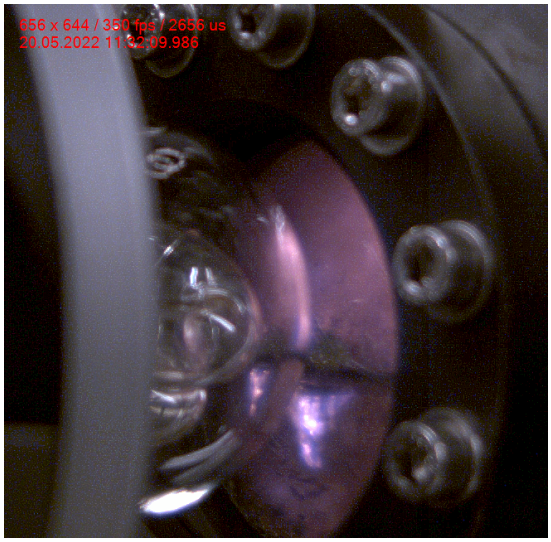

(f) Flame termination phase - 800 ms

Figure 20: Development of combustion using photo ignition at ϕ=0.8 and p=4 bar and sample weight of 36 mg, in experiment 18.

The first image, Fig. 20a, shows that the camera flash is placed right next to the optical access of the combustion chamber. The sample containing CNTs and ferrocene is situated at the glass plate, right within the quartz glass. The flash is triggered, and the first ignition of the sample is seen inside the combustion chamber.

After the flash, a large portion of the sample is ignited, which is seen by the glowing points in Fig. 20c. This happens approximately 35 ms after the flash is triggered. Additionally, the ignited particles eventually starting the combustion is seen at the lower part of the image. It is several noticeably larger collections of glowing particles. The air-methane mixture is ignited by these collections soon after, seen in Fig. 20d.

An interesting observation to be made, is that the combustion starts beneath the glass plate, which is on the other side of where the sample was initially placed. This could be caused by several reasons. One of them could be that the synthetic air stream injected onto the particles creates a vortex which moves particles from the upper side of the plate to the lower. Another potential reason could be that the injected synthetic air forces the particles between the quartz glass and the glass plate. This could easily be investigated using the high speed camera, but due to time constraints, such an experiment was not conducted.

The images captured from the video made for the successful photo ignition shows a bright chamber for the most of the combustion. This is seen in Fig. 20e.

Fig. 20f shows that approximately 800 ms after the flash is triggered, the flame within the combustion chamber has been terminated. The pressure and temperature curve for this specific combustion is shown in Fig. 21. In order to set a suitable start and end for the different phases, the ignition delay ends at 5% of the peak pressure, while the flame propagation phase ends at 95% of the peak pressure. This is in line with what was discussed in Ch. 2.4.

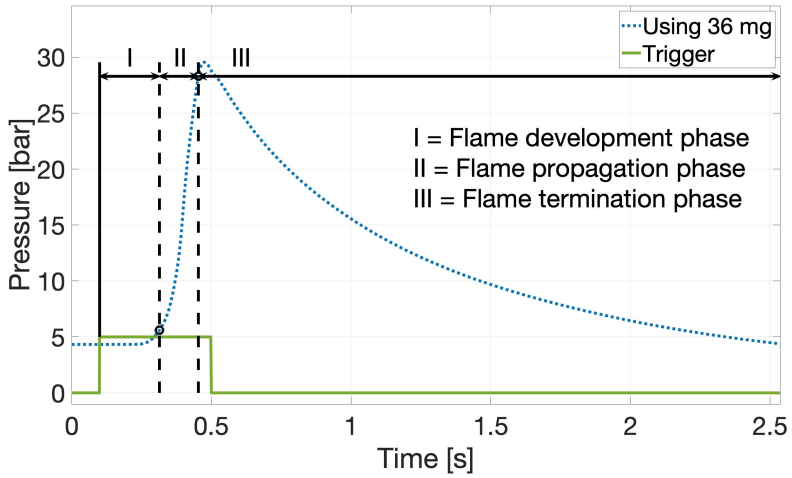

Figure 21: Combustion phases using photo ignition at p=4 bar and ϕ=0.8. Pressure development is given in absolute pressure.

The flame propagation phase is shorter than the flame development phase. This means that the flame front propagates through most of the air-methane mixture within the chamber, faster than the the interval needed to create a noticeably pressure increase due to combustion. Another interesting aspect which is evident in Fig. 21, is that the flame termination phase is much longer compared to the first two stages. However, this is logical, due to the heat transfer to the walls, which decreases the pressure within the chamber, takes longer time compared to the combustion. The decrease in turbulence also contributes to this fact.

As a result of successful ignition being achieved, the limits for the possibility of photo ignition had to be investigated. In order to conduct this investigation, it was decided to change the amount of the sample at a given pressure. The pressure needed to be altered to understand how the photo ignition depended on this physical property. The effect of the sample amount and pressure were explored for different equivalence ratios as well. Furthermore, it was explored how steady the combustion within the chamber did produce results for the relevant pressures and equivalence ratios using SI. Results from these tests are shown in Fig. 22.

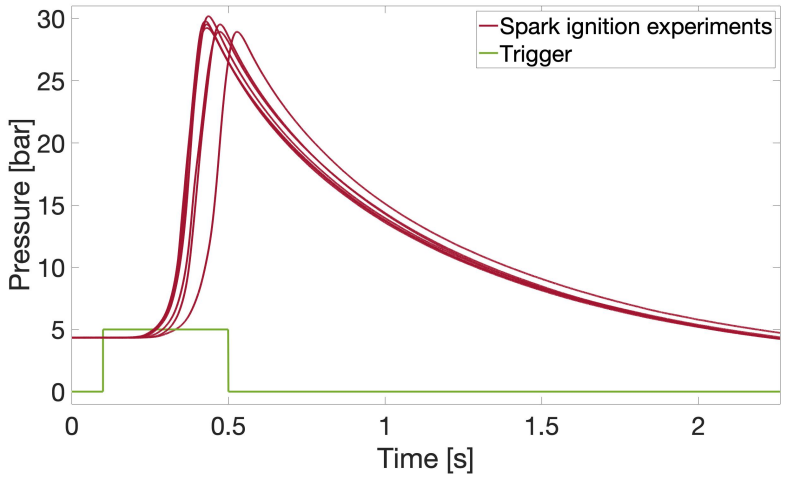

Figure 22: 7 experiments conducted for combustion using spark ignition at p=4 bar and ϕ=0.8. Pressure developments are given in absolute pressure.

As only 7 experiments were conducted using SI at p=4 bar and ϕ=0.8, it is difficult to say how repeatable the results are. In Fig. 22, a notable variation in the ignition delay is evident for several of the experiments. Additionally, the peak pressure also varies. Since there was not much time left when the successful photo ignition was obtained, it was decided that it was more important to do different experiments, rather than to conduct a lot of similar experiments in order to find the error margin. Fig. 22 showed that the results obtained in the combustion experiments in this thesis would contain an amount of uncertainty, due to variation of ignition delays and peak pressures. This could be due to for example imperfections in the experimental rig or coincidences.

Experiments 18-23 were conducted in order to study the effect of varying the sample amount at ϕ=0.8 and ϕ=0.7 using photo ignition. Only one experiment of each configuration was conducted, and the pressure developments does therefore represent some uncertainty. The results shown in Fig. 23 for the comparison between different p and ϕ will give an indication for which experimental configurations will give a successful ignition for the used setup, and how they compare to each other.

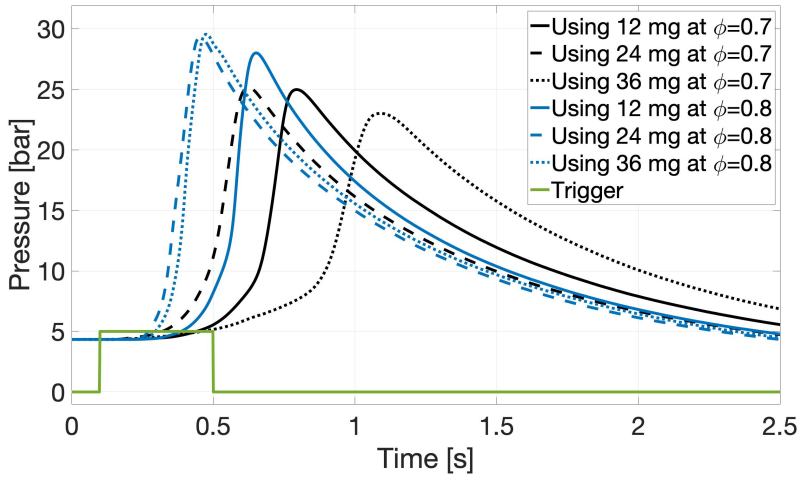

Figure 23: Photo ignition dependence on weight of CNTs/ferrocene sample and ϕ, at p=4 bar. Pressure developments are given in absolute pressure.

The results does imply some relationships between different weights of samples and equivalence ratios. Both the ignition delay, shown in the slower pressure rise, and the peak pressure are lower for the two of the experiments conducted at ϕ=0.7. This is expected, as the mass of methane in the combustion chamber is lower for these configurations. Hence, the flame will propagate slower due to the lack of fuel, which in turn increases the ignition delay. Additionally, the lack of methane leads to a lower temperature due to fewer chemical reactions which affects the peak pressure.

On the other hand, when only 12 mg of the sample was used at ϕ=0.8, the ignition delay is lower compared to the biggest amount of CNTs and ferrocene at ϕ=0.7. This could be caused by fewer ignition points within the combustion chamber, due to a lower amount of the ignited sample. Meanwhile, the peak pressure is highest for the richest ϕ, which is understandable, due to the larger amount of methane within the chamber. The lower ignition delay for the leanest equivalence ratio could also be due to errors or coincidences in the conducted experiments.

Furthermore, it was important to compare the pressure peak and ignition delay for photo and spark ignition. Such a comparison for an equivalence ratio of 0.8 is shown in Fig. 24. On the other hand, as there was not obtained any successful SI at an ϕ=0.7, a comparison between the spark and photo ignition could not be conducted for this equivalence ratio.

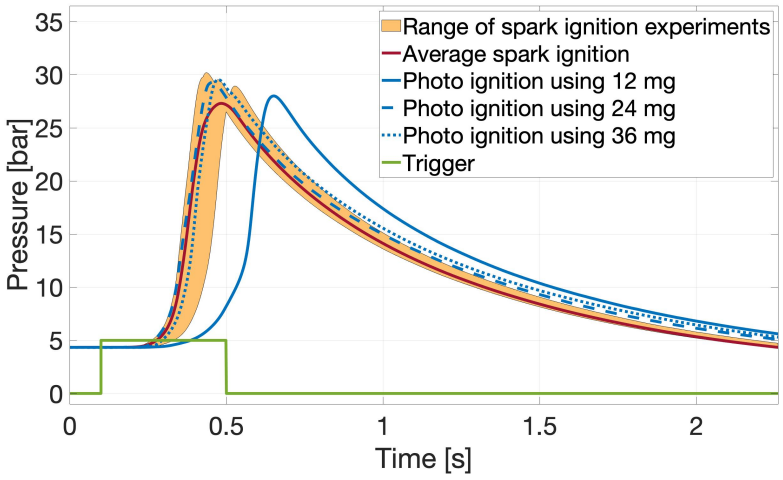

Figure 24: Comparison of photo ignition and average spark ignition at p=4 bar and ϕ=0.8. Pressure developments are given in absolute pressure.

From Fig. 24, it is noticeable that the spark and photo ignition for sample amounts of 24 mg and 36 mg are relatively similar. On the contrary, when only 12 mg of the sample is used, the ignition delay increases noticeably, whereas the pressure peak decreases by a relatively small amount. In order to conduct a comparison of the ignition delays and peak pressures for this experimental configuration, two variables are defined in Eq. 7.

$$\begin{aligned} \Delta \mathrm{P_{SI}} &= \frac{\text{Peak pressure for photo ignition}}{\text{Peak pressure for spark ignition}} - 1 \\ \Delta \mathrm{t_{SI}} &= \frac{\text{Ignition delay for photo ignition}}{\text{Ignition delay for spark ignition}} - 1 \end{aligned} \tag{7}$$

The comparison between spark and photo ignition is shown in Table 8, using the two aforementioned variables.

Table 8: Comparison of peak pressure and ignition delay for combustions at ϕ=0.8 and p=4 bar. Pressures are given as pressure above the absolute pressure.

Ignition type	Sample amount	Ignition delay	$\Delta \mathrm{t_{SI}}$	Peak pressure	$\Delta \mathrm{P_{SI}}$
Spark		195.5 ms		22.96 bar	
Photo	12 mg	321.0 ms	64.2%	23.67 bar	3.10%
Photo	24 mg	187.0 ms	-4.35%	24.96 bar	8.71%
Photo	36 mg	214.2 ms	9.57%	25.20 bar	9.76%

As seen in the table above, the ignition delay for the photo ignition is shorter using a sample amount of 24 mg, compared to SI. Meanwhile, the ignition delay increases using other weights of CNTs and ferrocene. However, as seen in Fig. 24, the uncertainty of taking the average of all the SI experiments is too large in order to conclude with anything. Therefore, the statistical data should be expanded to be able to do a proper comparison of the SI and the photo ignition.

After having investigated the effect of varying the amounts of sample used for igniting the mixture, the pressure dependence needed to be explored. Experiments 24-29 shows the configurations used in order to understand this matter. An interesting result observed for these experiments is that successful photo ignition is obtained for pressures down to 2 bar for ϕ=0.7. Meanwhile, for ϕ=0.8, a pressure of 3 bar is required in order for photo ignition to be obtained. This is peculiar, since Fig. 23 shows that a better combustion, in terms of pressure development, is achieved using an equivalence ratio of 0.8. Therefore, one would assume that this is the air-methane mixture connected to the smallest MIE. This is due to more methane being available close to the CNTs and ferrocene sample, which is needed for the combustion. Photo ignition only occurring for p=2 bar at ϕ=0.7 could indicate that the access to air is more important than the amount of methane near the burning particles. On the other hand, this would mean that a faster pressure increase should be expected for the case using a smaller equivalence ratio, which is not the case, as seen in Fig. 23.

Consequently, the pressure development could be insignificant for the limit of successful ignition. Since the flame development and propagation phase are two separate stages, which depends on different factors, they could be independent of each other. For example, a short ignition delay does not have to directly lead to the combustion finishing in a short amount of time. Therefore, it could be more effective to investigate the ignition of the mixtures, rather than the flame propagation phase, in order to assess the ignition process. On the other hand, the unsuccessful ignition at 2 bar for ϕ=0.8, as opposed to the successful for ϕ=0.7, could be due coincidences or errors being made in the execution of the experiment. As previously mentioned, only one experiment was conducted for each configuration. Therefore, some uncertainties in the results are expected.

In addition to investigating the pressure dependence and variation within a number of different equivalence ratios, the upper and lower limit of the ϕ also needed to be explored. Experiments 30, 31 and 33 were conducted using an equivalence ratio of 0.9. Even though both ϕ=0.7 and ϕ=0.8 were configurations which led to successful photo ignition at an initial pressure of 4 bar, the air-methane mixture did not successfully ignite at ϕ=0.9. If this was not caused by coincidences or errors, it had to be caused by a lack of air next to the particles, due to the equivalence ratio being the only parameter changed from experiments 20 and 27. A particular thing to note as well, in Fig. 5, successful ignition of a similar air-methane mixture at ϕ=1.0 was achieved in previous studies [8].

Unlike the experiments conducted in this project, Carlucci et al. used a sample homogeneously dispersed within the combustion chamber. Additionally, the Xe flash was mounted within the chamber. As shown in Eq. 6, oxygen is required for the methane to release energy through chemical reactions. Since the CNTs consist of carbon, and reacts with oxygen in order to produce carbon dioxide and carbon monoxide, a lack of oxygen could be present next to the burning particles [32]. Using a homogeneously dispersed sample could affect the air-methane mixture surrounding the particles less, when compared to using a pile. Although having a pile next to the light source eases the ignition of the sample of CNTs and ferrocene, it is possible that igniting the air-methane mixture becomes more difficult.

As no successful ignition was obtained using an equivalence ratio of ϕ=0.9, it was concluded that the upper limit for photo ignition was at ϕ=0.8 and p=3 bar, for this experimental setup. The lower limit was investigated using ϕ=0.6, where the rest of the configurations are shown in experiment 34 in Table 7. Similar to the tests conducted using an equivalence ratio of 0.9, no successful photo ignition was achieved for this ϕ. As a combustion was obtained using ϕ=0.7 and p=2 bar in experiment 25, it was a bit unexpected that no ignition occurred when testing an equivalence ratio of 0.6 at an initial pressure of 4 bar. This is due to the MIE decreasing with increasing initial combustion chamber pressure, as discussed in Ch. 2.4.

However, this result could also point to the MIE being more dependent on the ϕ compared to the p. This could explain why experiment 25 produced a successful photo ignition, while experiment 34 did not. Additionally, since there is less methane in the combustion chamber for ϕ=0.6, coincidences could decide if a successful photo ignition is achieved for this equivalence ratio. Since the mixing of the air and methane would not be flawless, conducting more experiments for this configuration could lead to a photo ignition being obtained. Most probably, by having better mixing or a small portion of the chamber being richer close to the sample, the air-methane mixture could be ignited.

One of the last experiments conducted was to decide if the substitution of nitrogen with synthetic air was decisive for the successful photo ignition experiments. In order to investigate this matter, the nitrogen supply was once more attached to the circuit originally used for injecting the samples. The rest of the experimental configuration is shown in experiment 38 in Table 7. Successful photo ignition was obtained for this experiment. A comparison of the pressure development for this setup with the equal configuration used for the synthetic air injection is shown in Fig. 25

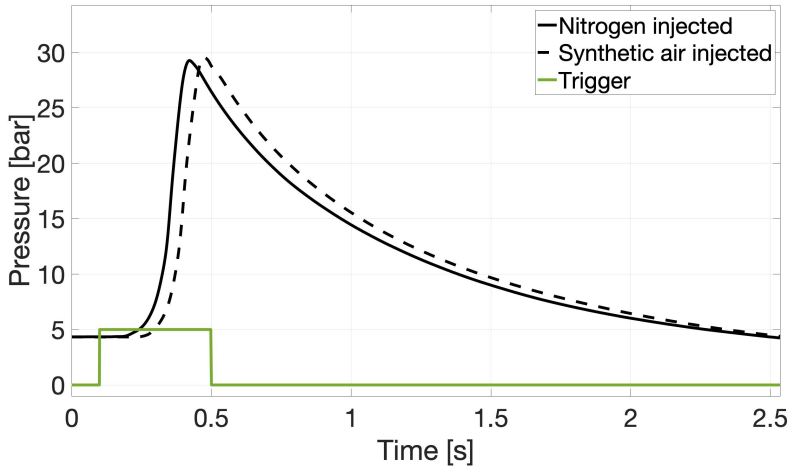

Figure 25: Comparison of photo ignition using injection of synthetic air and nitrogen at p=4 bar and ϕ=0.8. Pressure developments are given in absolute pressure.

As seen in the mentioned figure, there are some differences between injection of synthetic air and nitrogen. There are both higher pressure peak and ignition delay using synthetic air, but the differences are no larger than the variation between equal experiments using a spark plug, as reported in Fig. 22. Therefore, it is hard to say if there is a difference between injecting nitrogen or synthetic air, since the deviation could come from coincidences or errors made when conducting the experiment.

Nevertheless, since photo ignition was achieved, the hypothesis mentioned earlier stating that a lack of oxygen is the main reason for the unsuccessful ignitions, was rejected. Therefore, the combustion of the air-methane mixture initiated by the glowing sample, were thought to be due to the spreading of the particles. Due to time constraints, this experiment with a configuration listed in experiment 39 in Table 7, was not conducted.

As the sample containing CNTs and ferrocene would be quasi-homogeneously dispersed in a working ICE, an experiment injecting the particles through the tube was conducted. The configuration is listed in experiment in 40 in Table 7. Since a lower pressure difference between the injected synthetic air and the initial chamber pressure was used, compared to previous injection tests, a new ignition delay had to be used. Again, due to time constraints, a new experiment using the high speed camera was not conducted, in order to test the injection at the new pressure difference. However, as seen in Fig. 17b, an injection analysis was already done for a pressure difference of 1 bar and a sample weight of 24 mg. Therefore, the already mentioned MATLAB script was used to calculate the optimum ignition delay for this configuration, which was equal to approximately 160 ms.

Firstly, an attempt was made using the fan, in order to have the sample quasi-homogeneously dispersed within the combustion chamber. The ignition delay was set to 160 ms and the process was filmed. However, no successful photo ignition was obtained for this configuration. Additionally, no glowing particles was seen in the video. On the other hand, this could be caused by the camera only filming a small part of the combustion chamber, so particles could have been ignited further into the chamber. Another possible explanation could be that the ignition delay was incorrect, due to the video being used in order to decide the timing, was with the fan turned off.

Anyway, it was decided to reduce the turbulence, by turning the fan off, in order to mimic the injection achieved in Fig. 17b. The configuration for this test is shown in experiment 41. Unfortunately, the experiment was not conducted due to time constraints.

Several additional experiments were not conducted due to time constraints. An investigation of photo ignition at the configuration listed in experiment 31, would have given a complete understanding of the combustion process at ϕ=0.9. This is also the case for experiment 35 to 37, where an equivalence ratio of 0.6 would be used, combined with an initial pressure from 4.5 bar to 2.5 bar. However, since no successful ignition was achieved at 5.5 bar for both aforementioned equivalence ratios, it is expected that no photo ignition were to be obtained for these experiments. This is due to the MIE for the air-methane mixture decreasing with increasing pressures, as mentioned in Ch. 2.4.

5 Conclusion

In order to investigate which Xe lamps had the required attributes for igniting the samples of CNTs and ferrocene, several types were tested. It was found that the camera flash delivered noticeably more luminous energy compared to the Xe lamps driven by the standalone circuit board. However, some of the light source configurations, such as the two linear 50 J lamps in series, showed promising results. Unfortunately, the circuit board short circuited during operation. Since the camera flash was obtained when the new circuit boards arrived, no further investigation was made for the other light sources, due to the high luminous energy from the camera flash.

Most importantly, successful photo ignition of an air-methane mixture has been achieved through this work. For the first time, to the authors' knowledge, a light source placed outside a combustion chamber has managed to initiate a combustion within the chamber. Photo ignition has occurred at leaner conditions compared to SI for this experimental setup.

In addition to combustion being achieved at lean mixtures, higher peak pressures and shorter ignition delays occurred using a specific sample of CNTs and ferrocene, as the ignition agent. This would enhance the ICEs performance, which proves the interesting concept of the idea. Several experiments were conducted in order to find the outer limits of the photo ignition for the combustion chamber used in this project. The configurations for the upper and lower limit for successful ignition, are respectively listed in experiments 18 and 25 in Table 7.

Due to time constraints, only one single experiment was conducted for each configuration, therefore the results do contain an amount of uncertainty. Both the peak pressures and ignition delays, in addition to the limits for successful combustion, could be changed if more experiments were to be conducted. Nevertheless, the results in this thesis gives an indication of which experimental configurations would yield a successful photo ignition of the air-methane mixture. Additionally, it has been proven that it is possible to do so, with a light source placed outside of the combustion chamber.

As mentioned in the objectives of this thesis in Ch. 1.2, it was desired to conduct experiments using photo ignition within the OACIC. Additionally, an investigation using different mixtures within the combustion chamber, such as ammonia or hydrogen instead of methane would have been interesting. Unfortunately, time constraints limited the research to the experiments reported in this thesis.

6 Further work

Since the limits for successful ignition of the air-methane mixture have been indicated, combined with a fully functionally combustion chamber and light source, further experiments should be conducted. As there was only conducted one single experiment for each configuration in this thesis, a more extensive investigation of the possibility of successful photo ignition should be conducted. The focus should be centered around and within the limits found in this thesis. By doing a larger number of experiments at each of these configurations, a greater understanding of the limits would be obtained. Additionally, a statistical investigation could be conducted.

Consequently, when the photo ignition using the glass plate is fully understood, further experimental work should focus on injecting the sample of CNTs and ferrocene into the combustion chamber. Firstly, one should investigate the injection process at the experimental configuration which is shown to most consistent achieve successful photo ignition of the air-methane mixture. This is done using a high speed camera, in order to obtain the desired flash ignition delay.

Secondly, a thorough investigation of different experimental configurations should be conducted, to gain knowledge of the possibility of photo ignition using a quasi-homogeneously dispersed sample. It would be wise to start with ignition of the sample which is injected and directed towards the optical access and the light source. When successful photo ignition is achieved using this experimental setup, the fan should be used to quasi-homogeneously disperse the particles throughout the combustion chamber, before triggering the Xe flash.

Finally, as successful photo ignition of the air-methane is achieved for dispersed particles, ammonia should replace methane as the fuel. However, as ammonia requires higher chamber pressures compared to methane, no successful photo ignition will be expected using the static combustion chamber. Therefore, the experiments using an air-ammonia mixture should be conducted using the OACIC.

Furthermore, another light source than the Xe flash has to be investigated, due to its limitations regarding frequency of the flashes. The camera flash could be used in order to show a proof of concept, but in order to prove that this idea would work in a real engine, another light source should be used.

References

[1] J. E. Abboud, N. Jiang, Z. Zhang, S. Roy, and J. R. Gord. Spatial and temporal control of on-demand propane–air flame ignition by active photothermal effect of aluminum nanoenergetics. *Combustion and Flame*, 160(9):1842–1847, Sept. 2013.

[2] P. Ajayan, M. Terrones, A. Guardia, V. Huc, N. Grobert, B. Wei, H. Lezec, G. Ramanath, and T. Ebbesen. Nanotubes in a Flash–Ignition and Reconstruction. *Science (New York, N.Y.)*, 296:705, May 2002.

[3] M. Aziz, A. T. Wijayanta, and A. B. D. Nandiyanto. Ammonia as Effective Hydrogen Storage: A Review on Production, Storage and Utilization. *Energies*, 13(12):3062, Jan. 2020. Number: 12 Publisher: Multidisciplinary Digital Publishing Institute.

[4] A. Badakhshan and S. Danczyk. Ignition of Nanoparticles by a Compact Camera Flash. Technical report, AIR FORCE RESEARCH LAB EDWARDS AFB CA AEROSPACE SYSTEMS DIRECTORATE, Sept. 2014. Section: Technical Reports.

[5] A. Berkowitz and M. Oehlschlaeger. The photo-induced ignition of quiescent ethylene/air mixtures containing suspended carbon nanotubes. *Proceedings of The Combustion Institute - PROC COMBUST INST*, 33:3359–3366, Dec. 2011.

[6] B. Bockrath, K. Johnson, D. Sholl, B. Howard, C. Matranga, W. Shi, and D. Sorescu. Igniting Nanotubes with a Flash. *Science (New York, N.Y.)*, 297:192–3; author reply 192, Aug. 2002.

[7] N. Braidy, G. A. Botton, and A. Adronov. Oxidation of Fe Nanoparticles Embedded in Single-Walled Carbon Nanotubes by Exposure to a Bright Flash of White Light. *Nano Letters*, 2(11):1277–1280, Oct. 2002. Publisher: American Chemical Society (ACS).

[8] A. P. Carlucci and L. Strafella. Air-methane Mixture Ignition with Multi-Walled Carbon NanoTubes (MWCNTs) and Comparison with Spark Ignition. *Energy Procedia*, 82:915–920, Dec. 2015.

[9] A. P. Carlucci, P. Visconti, P. Primiceri, L. Strafella, A. Ficarella, and D. Laforgia. Photo-Induced Ignition of Different Gaseous Fuels Using Carbon Nanotubes Mixed with Metal Nanoparticles as Ignitor Agents. *Combustion Science and Technology*, 189(6):937–953, June 2017. Publisher: Taylor & Francis _eprint: https://doi.org/10.1080/00102202.2016.1256880.

[10] B. Chehroudi. Minimum ignition energy of the light-activated ignition of single-walled carbon nanotubes (SWCNTs). *Combustion and Flame*, 159:753–756, Feb. 2012.

[11] B. Chehroudi, G. L. Vaghjiani, and A. D. Ketsdever. Method for distributed ignition of fuels by light sources, Apr. 2009.

[12] H. Chen and G. Diebold. Chemical generation of acoustic waves: A giant photoacoustic effect. *Science*, 270(5238):963, Nov. 1995. Num Pages: 963 Place: Washington, United States Publisher: The American Association for the Advancement of Science.

[13] G. Cui, W. Zeng, Z. Li, Y. Fu, H. Li, and J. Chen. Experimental study of minimum ignition energy of methane/air mixtures at elevated temperatures and pressures. *Fuel*, 175:257–263, July 2016.

[14] S. Demesoukas, C. Caillol, P. Higelin, A. Boiarciuc, and A. Floch. Near wall combustion modeling in spark ignition engines. Part A: Flame–wall interaction. *Energy Conversion and Management*, 106:1426–1438, Dec. 2015.

[15] R. K. Eckhoff. Gas and Vapor Cloud Explosions. In *Explosion hazards in the process industries*. Gulf Professional Publishing, Amsterdam, Netherlands, second edition. edition, 2016.

[16] D. Erdemir and I. Dincer. A perspective on the use of ammonia as a clean fuel: Challenges and solutions. *International Journal of Energy Research*, 45(4):4827–4834, 2021. _eprint: https://onlinelibrary.wiley.com/doi/pdf/10.1002/er.6232.

[17] P. R.-F. H. Jørgensen. To be published. Master's thesis, NTNU, Trondheim, June 2022.

[18] B. Kang, Y. Dai, S. Chang, and D. Chen. Explosion of single-walled carbon nanotubes in suspension induced by a large photoacoustic effect. *Carbon*, 46:978–981, May 2008.

[19] C. D. Malec, N. H. Voelcker, J. G. Shapter, and A. V. Ellis. Carbon nanotubes initiate the explosion of porous silicon. *Materials Letters*, 64(22):2517–2519, Nov. 2010.

[20] H. Nakamura and M. Shindo. Effects of radiation heat loss on laminar premixed ammonia/air flames. *Proceedings of the Combustion Institute*, 37(2):1741–1748, Jan. 2019.

[21] P. R. Orszag. Huge Container Ships' Biggest Problem Is Emissions. *Bloomberg.com*, Mar. 2021.

[22] R. Paschotta. Coherence.

[23] R. Paschotta. Fluence.

[24] R. Paschotta. Pyroelectric Detectors.

[25] P. Primiceri, R. de Fazio, L. Strafella, A. P. Carlucci, and P. Visconti. Photo-induced ignition phenomenon of carbon nanotubes by Xenon pulsed light: Ignition tests analysis, automotive and new potential applications, future developments. *Journal of Applied Research and Technology*, 15(6):609–623, Dec. 2017.

[26] W. W. Pulkrabek. Combustion. In *Engineering Fundamentals of the Internal Combustion Engines*. Pearson, second edition, 2004.

[27] W. W. Pulkrabek. Fluid Motion within Combustion Chamber. In *Engineering Fundamentals of the Internal Combustion Engines*. Pearson, second edition, 2004.

[28] W. W. Pulkrabek. Thermochemistry and Fuels. In *Engineering Fundamentals of the Internal Combustion Engines*. Pearson, second edition, 2004.

[29] J. Smits, B. Wincheski, M. Namkung, R. Crooks, and R. Louie. Response of Fe powder, purified and as-produced HiPco single-walled carbon nanotubes to flash exposure. *Materials Science and Engineering: A*, 358:384–389, Oct. 2003.

[30] S.-H. Song, C.-G. Cho, S.-M. Park, H.-I. Park, and H.-J. Ryoo. Design and Implementation of Novel Series Trigger Circuit for Xenon Flash Lamp Driver. *IEEE Transactions on Plasma Science*, 46(10):3584–3590, Oct. 2018. Conference Name: IEEE Transactions on Plasma Science.

[31] S. Sousa, T. Peixoto, R. Santos, A. Lopes, M. Paiva, and A. Marques. Health and Safety Concerns Related to CNT and Graphene Products, and Related Composites. *Journal of Composites Science*, 4:106, Aug. 2020.

[32] N. N. Sysoev, A. I. Osipov, A. V. Uvarov, and O. A. Kosichkin. Flash ignition of a carbon nanotube. *Moscow University Physics Bulletin*, 66(5):492–494, Oct. 2011.

[33] S. Trewartha, R. Appleby, J. Gascooke, and J. Shapter. Mechanism of Laser Initiated Carbon Nanotube Ignition. *Propellants, Explosives, Pyrotechnics*, 43, July 2018.

[34] S. H. Tseng, N. H. Tai, W. K. Hsu, L. J. Chen, J. H. Wang, C. C. Chiu, C. Y. Lee, L. J. Chou, and K. C. Leou. Ignition of carbon nanotubes using a photoflash. *Carbon*, 45(5):958–964, Apr. 2007.

[35] United Nations. Paris agreement. Technical report, Dec. 2015.

[36] P. Visconti, P. Primiceri, R. de Fazio, A. P. Carlucci, S. E. Mazzetto, and G. Mele. Improved Photo-Ignition of Carbon Nanotubes/Ferrocene Using a Lipophilic Porphyrin under White Power LED Irradiation. *Materials (Basel, Switzerland)*, 11(1):E127, Jan. 2018.

[37] P. Visconti, P. Primiceri, R. De fazio, L. Strafella, A. Ficarella, and A. P. Carlucci. Light-Induced ignition of Carbon Nanotubes and energetic nano-materials: a review on methods and advanced technical solutions for nanoparticles-enriched fuels combustion. *REVIEWS ON ADVANCED MATERIALS SCIENCE*, 59:26–46, Mar. 2020.

[38] P. Visconti, P. Primiceri, D. Longo, L. Strafella, P. Carlucci, M. Lomascolo, A. Cretì, and G. Mele. Photo-ignition process of multiwall carbon nanotubes and ferrocene by continuous wave Xe lamp illumination. *Beilstein Journal of Nanotechnology*, 8(1):134–144, Jan. 2017. Publisher: Beilstein-Institut.

Appendices

A Static combustion chamber

A.1 Setup

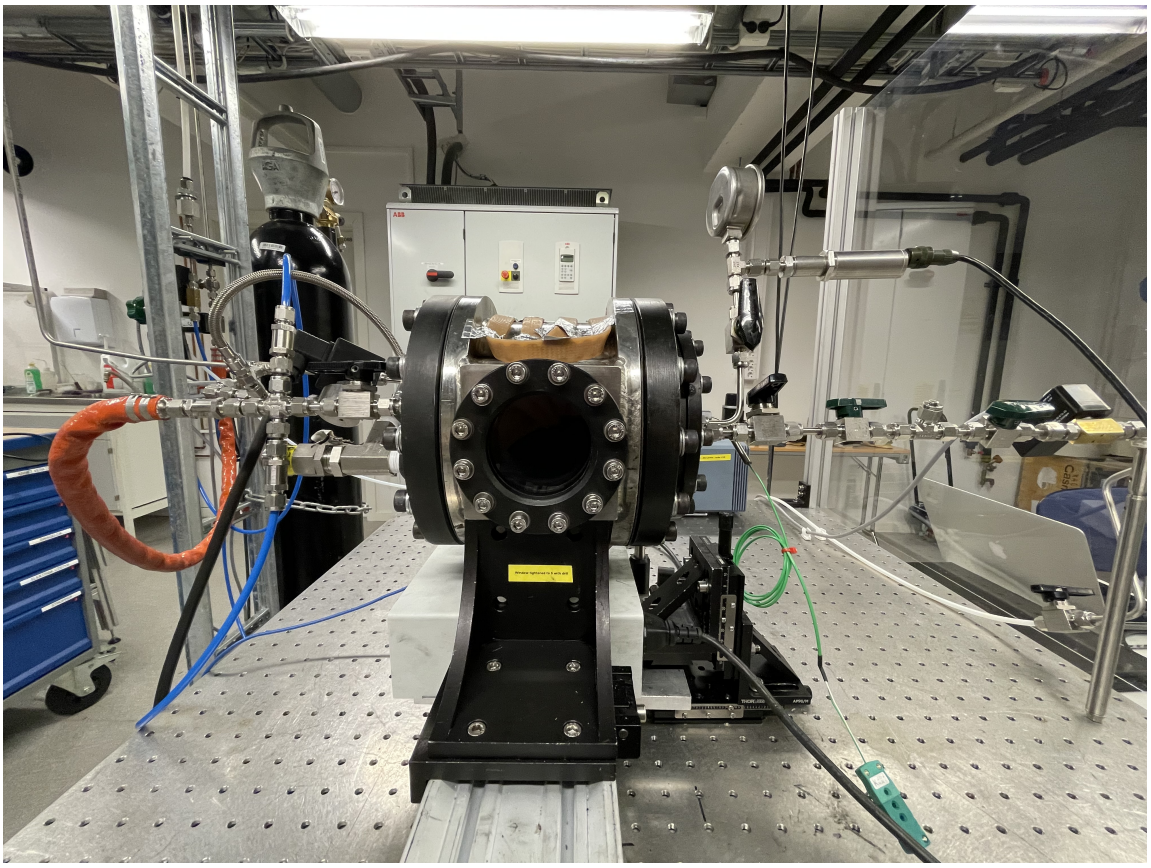

Figure 26: The static combustion chamber and its optical access.

A.2 Performance report

There will be some variations between the experiments conducted within the static combustion chamber. Table 9 and Table 10 are included to give an understanding of how some parameters varies within the same initial conditions, and for varying equivalence ratio, ϕ. One of the chosen parameters is the calculated ϕ. This provides an insight in the uncertainty of the equivalence ratio. The maximum incline of the pressure development is included to separate the rate at which the pressure grows for each experiment. Furthermore, peak pressure and temperature are there to explain the variation of the magnitude of the physical parameters. As mentioned in Ch. 1.2, there is a master's thesis focusing more on SI in this specific combustion chamber, which will discuss these variations in detail [17].

Table 9: Parameters obtained from SI experiments, conducted at p=4 bar and ϕ=0.8.

Targeted ϕ	Calculated ϕ	Max $\frac{dp}{dt}$	Peak pressure	Peak temperature
0.8	0.864	0.0238	26.49 bar	369.64 °C
0.8	0.804	0.0222	25.89 bar	341.92 °C
0.8	0.788	0.0220	25.49 bar	318.44 °C
0.8	0.744	0.0215	25.23 bar	331.38 °C
0.8	0.799	0.0212	25.22 bar	326.12 °C
0.8	0.809	0.0213	24.94 bar	313.72 °C
0.8	0.804	0.0198	24.62 bar	360.65 °C

Table 10: Parameters obtained from SI experiments, conducted at p=2 bar with a range of ϕ.

Targeted ϕ	Calculated ϕ	Max $\frac{dp}{dt}$	Peak pressure	Peak temperature
0.8	0.799	0.0316	15.16 bar	257.45 °C
0.9	0.888	0.0443	17.34 bar	275.59 °C
1.0	1.000	0.0537	18.77 bar	307.30 °C
1.1	1.100	0.0648	20.59 bar	325.97 °C
1.2	1.196	0.0711	21.24 bar	324.50 °C
1.3	1.299	0.0632	21.27 bar	362.85 °C
1.4	1.508	0.0537	20.80 bar	320.42 °C

B OACIC

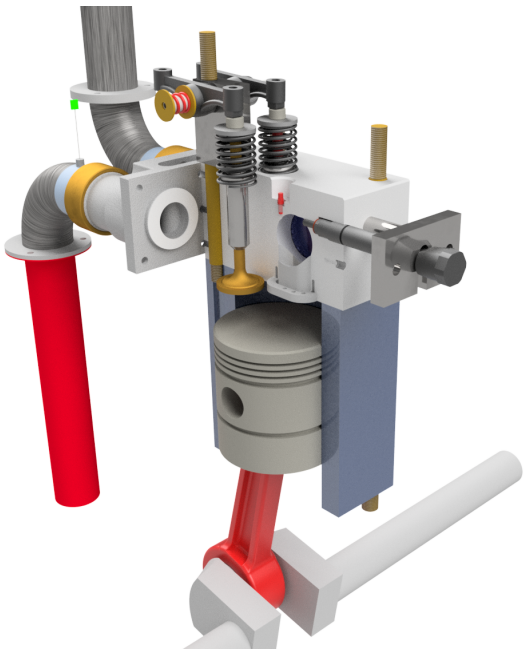

Figure 27: Illustration of the OACIC.

C Experimental setup for testing of camera flash

The flash tube of the camera flash is not symmetric and measurements was therefore conducted in order to understand how the luminous energy varies with the geometry of the flash tube. A pyroelectric sensor was mounted onto a manual rotation stage from Thorlabs, in order to accurately measure the angle between the sensor and camera flash when measuring the fluence. Fig. 28a is given to show which coordinates are used. It is to be interpreted that the camera flash tube is placed with the socket in the xy-plane.

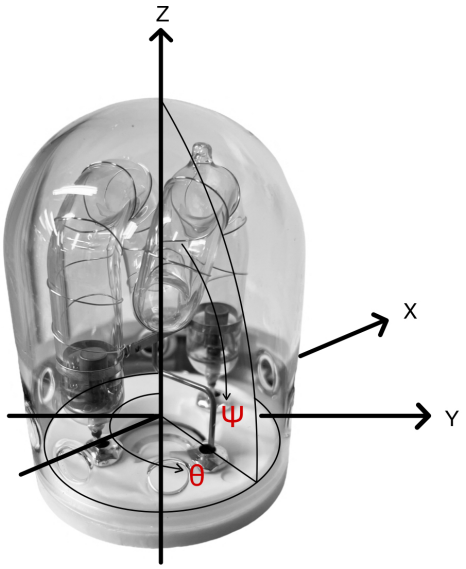

(a) Coordinates for investigating fluence from camera flash.

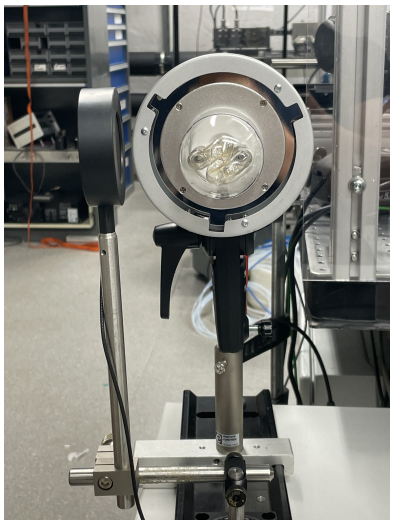

(b) Measuring fluence in θ-direction.

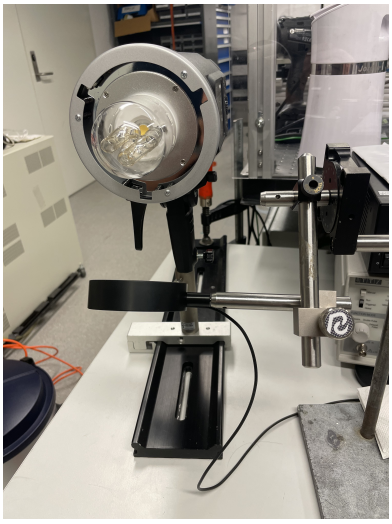

(c) Measuring fluence in ψ-direction in the yz-plane.

(d) Measuring fluence in ψ-direction in the xz-plane.

Figure 28: Experimental setup for testing of camera flash.

The measurements of the fluence for the configurations shown in Fig. 28, are given in Table 11. Since the camera flash is approximately symmetric in the θ-direction and ψ-directions, measurements are only conducted for 0°to 90°.

Table 11: Measurement of fluence at different angles for the camera flash tube.

Direction	Plane	Degrees	Fluence
θ		0°	$188.5\,\mathrm{mJ\,cm^{-2}}$
θ		30°	$199.4\,\mathrm{mJ\,cm^{-2}}$
θ		60°	$182.5\,\mathrm{mJ\,cm^{-2}}$
θ		90°	$183.7\,\mathrm{mJ\,cm^{-2}}$
ψ	xz	0°	$256.7\,\mathrm{mJ\,cm^{-2}}$
ψ	xz	30°	$226.2\,\mathrm{mJ\,cm^{-2}}$
ψ	xz	60°	$167.4\,\mathrm{mJ\,cm^{-2}}$
ψ	xz	90°	$161.2\,\mathrm{mJ\,cm^{-2}}$
ψ	yz	0°	$183.7\,\mathrm{mJ\,cm^{-2}}$
ψ	yz	30°	$215.5\,\mathrm{mJ\,cm^{-2}}$
ψ	yz	60°	$234.7\,\mathrm{mJ\,cm^{-2}}$
ψ	yz	90°	$255.2\,\mathrm{mJ\,cm^{-2}}$

As seen in Table 11, the fluence is maximized in the ψ-direction for the xz-plane at 0°and yz-plane

at 90°. This is as expected, due to the surface area of the flash tube being largest at this position. The mentioned measurement placements are at the top and the bottom of the light source.

D Script for computing optimum flash delay

```
clear all
clc

filename = 'test'; % Video file name
filetype = '.avi'; % Video file type

avgNumber = 5; % To filter out noice in image
numVideos = 1; % Number of videos
fps = 8000;    % Camera frames per second used to film the videos

% Preallocate memory
maximum = zeros(1,numVideos);
IND = maximum;
timing = IND;

%% Convert video to images and find image with most particles
for i = 1:numVideos
    v = VideoReader(strcat(strcat(filename,num2str(i)),filetype)); % Read video i
    j=1;
    while hasFrame(v) % Read frames as long as there is frames in the video
        frame = readFrame(v); % Read frame
        if j < 6

            % Find a background image the pixel values for the first
            % five images (before injection), in order to measure
            % change in pixel values
            background(j) = sum(sum(sum(frame)));

        else

            % Find the difference in pixel values between the current frame
            % and the average of the images before the injection
            sumCNT(j) = sum(sum(sum(frame)))/(sum(background)...
                /avgNumber);

        end
        j=j+1;
    end

    maximum(i) = min(sumCNT(avgNumber+1:end)); % Find frame with max pixels
    IND(i) = find(maximum(i) == sumCNT); % Find number of frame with max pixels
    timing(i) = 1000 * IND(i)/fps; % Optimum timing for flash [ms]
    storeImage = read(VideoReader(strcat(strcat(filename,num2str(i))...
```

```
        ,filetype)),IND(i)); % Read frame with max pixels
    imwrite(storeImage, [strcat(filename,num2str(i)) '.png']);  % Store frame with max pixels

    % Empty vectors
    sumCNT = [];
    background = [];
end
```

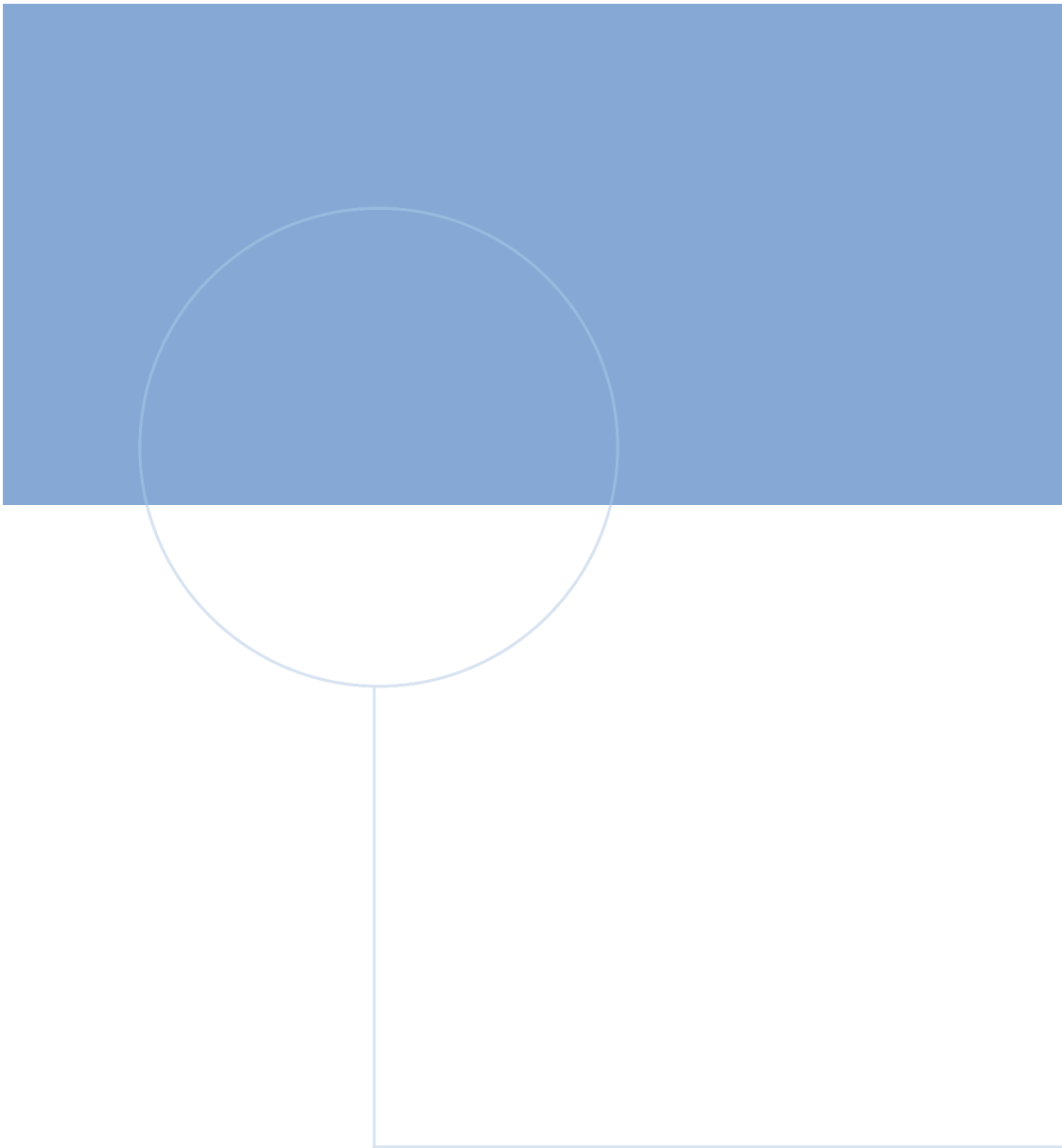

NTNU

Norwegian University of
Science and Technology